Abstracta

Ano XX - N. 02

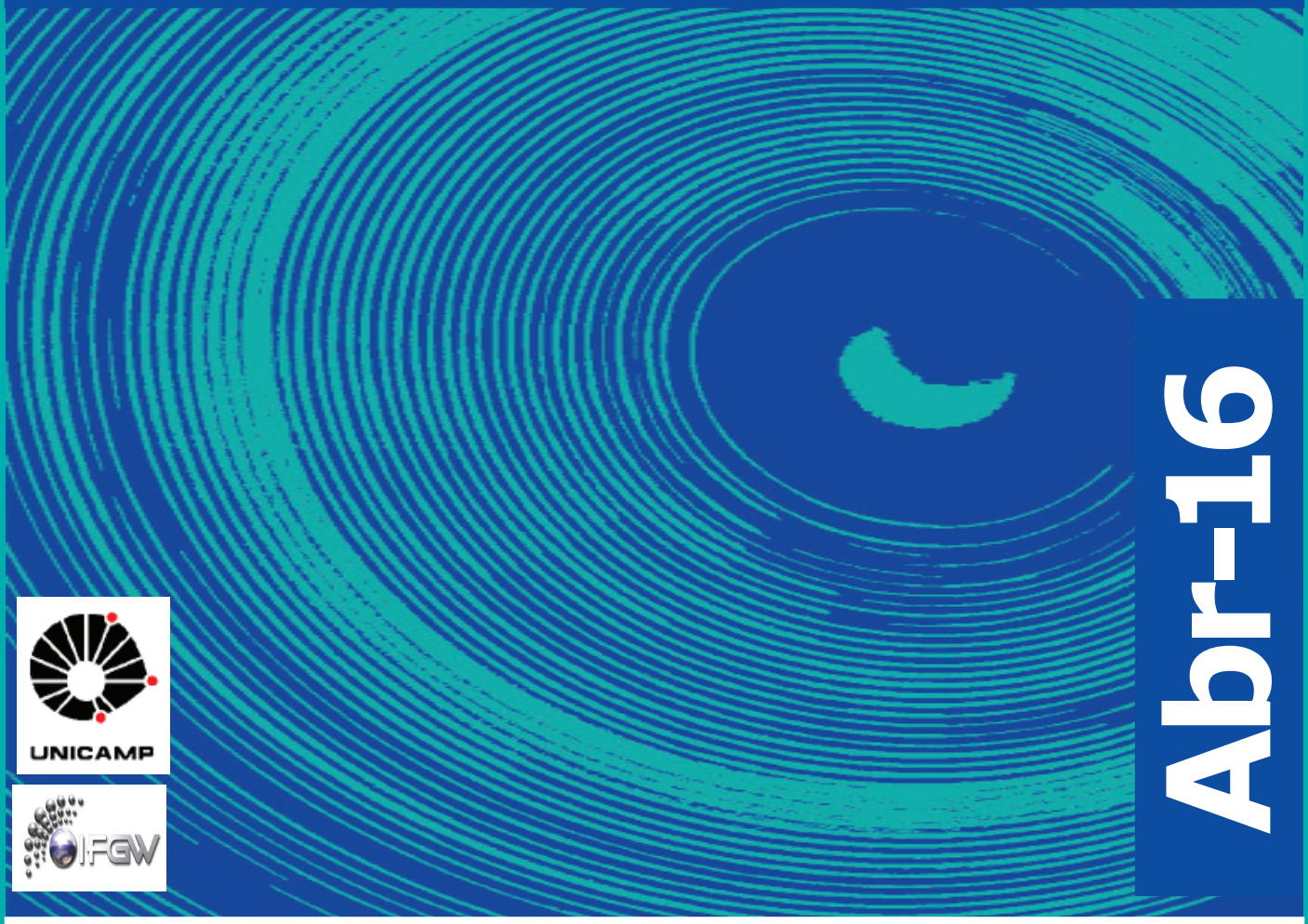

Abr-16

UNICAMP

IFGW

Trabalhos publicados em 2015 - P391-2015 à P396-2015

Trabalhos publicados em 2016 - P015-2016 à P101-2016

Livro publicado - L001-2016

Capítulos de Livros publicados- Ca001-2016 à Ca002-2016

Defesas de Dissertações do IFGW - D003-2016 à D007-2016

Defesas de Teses do IFGW - T005-2016 à T010-2016

Trabalhos publicados em 2015

[P391-2015] "Anticipating Economic Market Crises Using Measures of Collective Panic"

Harmon, D.; Lagi, M.; **de Aguiar, M. A. M.*; Chinellato, D. D.*;** Braha, D.; Epstein, I. R.; Bar-Yam, Y.

Predicting panic is of critical importance in many areas of human and animal behavior, notably in the context of economics. The recent financial crisis is a case in point. Panic may be due to a specific external threat or self-generated nervousness. Here we show that the recent economic crisis and earlier large single-day panics were preceded by extended periods of high levels of market mimicry-direct evidence of uncertainty and nervousness, and of the comparatively weak influence of external news. High levels of mimicry can be a quite general indicator of the potential for self-organized crises.

PLOS ONE 10[7], e0131871, 2015. DOI: 10.1371/journal.pone.0131871

[P392-2015] "Cerebral cortex involvement in Machado-Joseph disease"

de Rezende, T. J. R.*; D'Abreu, A.; Guimaraes, R. P.; Lopes, T. M.; Lopes-Cendes, I.; Cendes, F.; **Castellano, G.***; Franca, M. C., Jr.

Background and purposeMachado-Joseph disease (MJD/SCA3) is the most frequent spinocerebellar ataxia, characterized by brainstem, basal ganglia and cerebellar damage. Few magnetic resonance imaging based studies have investigated damage in the cerebral cortex. The objective was to determine whether patients with MJD/SCA3 have cerebral cortex atrophy, to identify regions more susceptible to damage and to look for the clinical and neuropsychological correlates of such lesions. MethodsForty-nine patients with MJD/SCA3 (mean age 47.713.0years, 27 men) and 49 matched healthy controls were enrolled. All subjects underwent magnetic resonance imaging scans in a 3 T device, and three-dimensional T1 images were used for volumetric analyses. Measurement of cortical thickness and volume was performed using the FreeSurfer software. Groups were compared using ancova with age, gender and estimated intracranial volume as covariates, and a general linear model was used to assess correlations between atrophy and clinical variables. ResultsMean CAG expansion, Scale for Assessment and Rating of Ataxia (SARA) score and age at onset were 72.1 +/- 4.2, 14.7 +/- 7.3 and 37.5 +/- 12.5years, respectively. The main findings were (i) bilateral paracentral cortex atrophy, as well as the caudal middle frontal gyrus, superior and transverse temporal gyri, and lateral occipital cortex in the left hemisphere and supramarginal gyrus in the right hemisphere; (ii) volumetric reduction of basal ganglia and hippocampi; (iii) a significant correlation between SARA and brainstem and precentral gyrus atrophy. Furthermore, some of the affected cortical regions showed significant correlations with neuropsychological data. ConclusionsPatients with MJD/SCA3 have widespread cortical and subcortical atrophy. These structural findings correlate with clinical manifestations of the disease, which support the concept that cognitive/motor impairment and cerebral damage are related in disease.

EUROPEAN JOURNAL OF NEUROLOGY 22[2], 277-+, 2015. DOI: 10.1111/ene.12559

[P393-2015] "Ferromagnetic Kondo behavior in UAuBi2 single crystals"

Rosa, P. F. S.*; Luo, Y. K.; Bauer, E. D.; Thompson, J. D.; **Pagliuso, P. G.*; Fisk, Z.***

We combine magnetization, pressure-dependent electrical resistivity, and heat capacity measurements to investigate the physical properties of the novel compound UAuBi2. Our single crystals, grown by the self-flux method, share the same tetragonal HfCuSi2-type structure as their Ce-based counterparts. UAuBi2 shows ferromagnetic ordering at T-c = 22.5 K, in contrast with the antiferromagnetic transition found in CeAuBi2 (T-N = 12 K) but closely related to UAuSb2 (T-c = 31 K). Despite the differences, all compounds display an easy axis of magnetization along the c axis and a large magnetocrystalline anisotropy. The heat capacity and pressure-dependent resistivity suggest that UAuBi2 exhibits moderately heavy-fermion behavior (gamma similar to 100 mJ/mol . K-2) with strongly localized 5f electrons. An intricate competition between crystalline electric field (CEF) effects and two anisotropic exchange interactions (J(RKKY)) persists in the 5f system, which leads to the striking difference between ground states. A systematic analysis of our macroscopic data using a mean-field model including anisotropic J(RKKY) interactions and the tetragonal CEF Hamiltonian allows us to extract the CEF scheme and the values of J(RKKY). Our results suggest a general trend in this family of compounds and shed light on the similarities and differences between 4f and 5f members.

PHYSICAL REVIEW B 92[10], 104425, 2015. DOI: 10.1103/PhysRevB.92.104425

[P394-2015] "Incorporation of Ca, P, and Si on bioactive coatings produced by plasma electrolytic oxidation: The role of electrolyte concentration and treatment duration"

Marques, I. D. V.; da Cruz, N. C.; **Landers, R.*;** Yuan, J. C. C.; Mesquita, M. F.; Sukotjo, C.; Mathew, M. T.; Barao, V. A. R.

The objectives of the present study were to produce bioactive coatings in solutions containing Ca, P, and Si by plasma electrolytic oxidation (PEO) on commercially pure titanium, to investigate the influence of different electrolytes concentration and treatment duration on the produced anodic films and to evaluate biocompatibility properties. The anodic films were characterized using scanning electron microscopy, energy-dispersive spectroscopy, atomic force microscopy, and x-ray diffraction and x-ray photoelectron spectroscopies. The surface energy and roughness were also evaluated. PEO process parameters influenced the crystalline structure formation and surface topography of the anodic films. Higher Ca content produced larger porous (volcanolike appearance) and thicker oxide layers when compared to the lower content. Treatment duration did not produce any topography difference. The treatment modified the surface chemistry, producing an enriched oxide layer with bioactive elements in the form of phosphate compounds, which may be responsible for mimicking bone surface. In addition, a rough surface with increased surface energy was generated. Optimal spreading and proliferation of human mesenchymal stem cells was achieved by PEO treatment, demonstrating excellent biocompatibility of the surface. The main finding is that the biofunctionalization with higher Ca/P on Ti-surface can improve surface features, potentially considered as a candidate for dental implants.

BIOINTERPHASES 10[4], 041002, 2015. DOI: 10.1116/1.4932579

[P395-2015] "Study of Cold Atmospheric Plasma Jet at the End of Flexible Plastic Tube for Microbial Decontamination"

Kostov, K. G.; Nishime, T. M. C.; **Machida, M.***; Borges, A. C.; Prysiazhnyi, V.; Koga-Ito, C. Y.

Recently, cold atmospheric plasmas have demonstrated very promising antimicrobial activity in vitro and in vivo including selective destruction of tumor cells.

However, the size and the rigidity of most plasma systems limit the clinical application for treatments in internal organs or regions with difficult access (e.g., mouth). Here, we report a device that allows ignition of cold He plasma jet at the tip of 1m long, 3.5 mm diameter, flexible plastic tube. It is connected to a dielectric enclosure where dielectric barrier discharge (DBD) is generated by a low-frequency AC power supply. A thin wire at floating potential put inside the plastic tube assists the formation of plasma jet at the downstream tube end. The flexible tube can be kept and manipulated by hand without electric shock and thus the plasma jet can be easily directed to a target. Variation of duty cycle of the applied voltage signal allows precise adjustment of the discharge power. The anti--microbial efficiency of plasma jet system with flexible tube was tested against fungus Candida albicans seeded on agar.

PLASMA PROCESSES AND POLYMERS 12[12], SI, 1383-1391, 2015. DOI: 10.1002/ppap.201500125

[P396-2015] "The influence of different silicon adhesion interlayers on the tribological behavior of DLC thin films deposited on steel by EC-PECVD"

Cemin, F.; Bim, L. T.; Menezes, C. M.; da Costa, M. E. H.; Baumvol, I. J. R.; **Alvarez, F.*;** Figueroa, C. A.

Diamond-like carbon (DLC) is a hydrogenated amorphous carbon (a-C:H) thin film material owing to its unique tribological properties that may open great opportunities for new applications. However, DLC presents low chemical affinity with metallic alloys and high intrinsic stress, prompting film delamination and poor adherence on the substrate. In the present work, we performed a systematic study about structural and tribological properties of a-C:H thin films grown on steel by introducing adhesive silicon-containing interlayers deposited at different processing temperatures and times. The studied bi-layers were deposited by electrostatic confinement plasma enhanced chemical vapor deposition (EC-PECVD) and were characterized by several techniques. The results showed that the adhesive interlayers produced from tetramethylsilane are chemically structured as a non-stoichiometry hydrogenated amorphous silicon carbide alloy (a-SiCx:H). Its structure, chemical composition and thickness are very dependent on deposition conditions. The thickness of the interlayers increases with deposition time and decreases with deposition temperature. The interlayer contains less hydrogen and silicon atoms at higher deposition temperatures, with enhanced formation of Si-C bonds in its structure. This last chemical event is correlated with the rise in the critical load values found for a-C:H film delamination when the a-SiCx:H interlayers are deposited from 573 K to 823 K. On the other hand, the interlayer contains less carbon atoms at higher deposition times, decreasing the critical load values for a-C:H film delamination when the a-SiCx:H interlayers are deposited from 5 min to 10 min.

SURFACE & COATINGS TECHNOLOGY 283, 115-121, 2015. DOI: 10.1016/j.surfcoat.2015.10.031

Trabalhos publicados em 2016

[P015-2016] "(3)(Lambda)Hand (3)((Lambda)over-bar)(H) over-bar production in Pb-Pb collisions at root s(NN)=2.76 TeV"

Adam, J.; Adamova, D.; Aggarwal, M. M.; **Chinellato, D. D.*; Dash, A.*; Takahashi, J.***; et al. ALICE Collaboration

The production of the hypertriton nuclei H-3(Lambda) and (3)((Lambda) over bar)(H) over bar has been measured for the first time in Pb-Pb collisions at root s(NN) = 2.76 TeVwith the ALICE experiment at LHC. The p(T)-integrated H-3(Lambda) yield in one unity of rapidity, dN/dy x B.R.((3 Lambda H -> 3He,pi-)) = (3.86 +/- 0.77(stat.) +/- 0.68(syst.)) x 10(-5) in the 0-10% most central collisions, is consistent with the predictions from a statistical thermal model using the same temperature as for the light hadrons. The coalescence parameter B-3 shows a dependence on the transverse momentum, similar to the B-2 of deuterons and the B-3 of He-3 nuclei. The ratio of yields S-3 = H-3(Lambda)/(He-3 x Lambda/p) was measured to be S-3 = 0.60 +/- 0.13(stat.) +/- 0.21(syst.) in 0-10% centrality events; this value is compared to different theoretical models. The measured S-3 is compatible with thermal model predictions. The measured H-3(Lambda) lifetime, tau = 181(-39)(+54)(stat.) +/- 33(syst.) psis in agreement within 1s with the world average value.

PHYSICS LETTERS B 754, 360-372, 2016. DOI: 10.1016/j.physletb.2016.01.040

[P016-2016] "A search for pair production of new light bosons decaying into muons"

Khachatryan, V.; Sirunyan, A. M.; Tumasyan, A.; **Chinellato, J.*; Tonelli Manganote, E. J.***; et al. CMS Collaboration

A search for the pair production of new light bosons, each decaying into a pair of muons, is performed with the CMS experiment at the LHC, using a dataset corresponding to an integrated luminosity of 20.7 fb(-1) collected in proton--proton collisions at center-of-mass energy of root s = 8 TeV. No excess is observed in the data relative to standard model background expectation and a model independent upper limit on the product of the cross section, branching fraction, and acceptance is derived. The results are compared with two benchmark models, the first one in the context of the next-to-minimal super-symmetric standard model, and the second one in scenarios containing a hidden sector, including those predicting a nonnegligible light boson lifetime.

PHYSICS LETTERS B 752, 146-168, 2016. DOI: 10.1016/j.physletb.2015.10.067

[P017-2016] "A two-layer approach to the coupled coherent states method"

Green, J. A.; **Grigolo, A.***; Ronto, M.; Shalashilin, D. V.

In this paper, a two-layer scheme is outlined for the coupled coherent states (CCS) method, dubbed two-layer CCS (2L-CCS). The theoretical framework is motivated by that of the multiconfigurational Ehrenfest method, where different dynamical descriptions are used for different subsystems of a quantum mechanical system. This leads to a flexible representation of the wavefunction, making the method particularly suited to the study of composite systems. It was tested on a 20-dimensional asymmetric system-bath tunnelling problem, with results compared to a benchmark calculation, as well as existing CCS, matching-pursuit/split-operator Fourier transform, and configuration interaction expansion methods. The two-layer method was found to lead to improved short and long term propagation over standard CCS, alongside improved numerical efficiency and parallel scalability. These promising results provide impetus for future development of the method for on-the-fly direct dynamics calculations.

JOURNAL OF CHEMICAL PHYSICS 144 [2] 024111, 2016. DOI: 10.1063/1.4939205

[P018-2016] "Angular analysis of the decay B-0 -> K*(0)mu(+) mu(-) from pp collisions at root s=8 TeV"

Khachatryan, V.; Sirunyan, A. M.; Tumasyan, A.; **Chinellato, J.*; Tonelli Manganote, E. J.***; et al. CMS Collaboration

The angular distributions and the differential branching fraction of the decay B-0 -> K*(892)(0)mu(+)mu(-) are studied using data corresponding to an integrated luminosity of 20.5 fb(-1) collected with the CMS detector at the LHC in pp collisions at root s = 8 TeV. From 1430 signal decays, the forward-backward asymmetry of the muons, the K*(892)(0) longitudinal polarization fraction, and the differential branching fraction are determined as a function of the dimuon invariant mass squared. The measurements are among the most precise to date and are in good agreement with standard model predictions.

PHYSICS LETTERS B 753, 424-448, 2016. DOI: 10.1016/j.physletb.2015.12.020

[P019-2016] "Anomalous temperature behavior of resistance in C1-xCox thin films grown by pulsed laser deposition technique"

Sergeenkov, S.; Cordova, C.; Cichetto, L., Jr.; de **Lima, O. F.***; Longo, E.; Araujo-Moreira, F. M.

We study the transport properties of C1-xCox thin films (with x = 0.1, 0.15 and 0.2) grown on Si substrate by pulsed laser deposition technique. The results demonstrate some anomalous effects in the behavior of the measured resistance R(T,x). More specifically, for 0 < T< T* range (with T* similar or equal to 220 K) the resistance is shown to be well fitted by a small polaron hopping scenario with R-h(T,x) proportional to exp{[T-0(x)/T](0.5)} and a characteristic temperature T-0(x) similar or equal to T-0(0)(1 - x) (with T-0(0) = 120 K). While for higher temperatures T* <T < T-C(x), the resistance is found to be linearly dependent on spontaneous magnetization M(T,x), viz. R-M(T,x)proportional to M(T,x), following the pattern dictated by electron scattering on cobalt atoms formed robust ferromagnetic structure with the Curie temperature T-C(x) obeying a percolation like law T-C(x)similar or equal to T-C(x(m))(x/x(m))(0.15) with T-C(x(m)) = 295 K and the maximum zero-temperature magnetization reaching M(0, x(m))=0.5 mu(B) per Co atom for x(m) = 0.2.

JOURNAL OF ALLOYS AND COMPOUNDS 667, 18-22, 2016. DOI: 10.1016/j.jallcom.2016.01.141

[P020-2016] "ARAPUCA a new device for liquid argon scintillation light detection"

Machado, A. A.*; Segreto, E.*

We present a totally innovative device for the detection of liquid argon scintillation light, that has been named ARAPUCA (Argon R&D Advanced Program at UniCAmp). It is composed of a passive light collector and of active devices. The latters are standard SiPMs that operate at liquid argon temperature, while the passive collector is based on a new technology, never explored in this field before. It is a photon trap, that allows to collect light with extremely high efficiency. The total detection efficiency of the device can be tuned by modifying the ratio between the area of the active devices (SiPM) and the area of the optical window. For example, it will allow to reach a detection efficiency at the level of 1% on a surface of 50 x 50 cm(2) with an active coverage of 2 x 2 cm(2) (two/three large area SiPM). It is also a cheap device, since the major part of its cost is represented by the active devices. For these reason this appears to be the ideal device for scintillation light detection in large Time Projection Chambers. With appropriate modifications it can be used also in next generation Dark Matter detectors.

JOURNAL OF INSTRUMENTATION 11, C02004, 2016. DOI: 10.1088/1748-0221/11/02/C02004

[P021-2016] "Azimuthal anisotropy of charged jet production in root s(NN)=2.76 TeV Pb-Pb collisions"

Adam, J.; Adamova, D.; Aggarwal, M. M.; C**hinellato, D. D.*; Dash, A.*; Takahashi, J.***; et al. ALICE Collaboration

We present measurements of the azimuthal dependence of charged jet production in central and semi-central root s(NN) = 2.76 TeV Pb-Pb collisions with respect to the second harmonic event plane, quantified as nu(ch)(2) (jet). Jet finding is performed employing the anti-k(T) algorithm with a resolution parameter R = 0.2 using charged tracks from the ALICE tracking system. The contribution of the azimuthal anisotropy of the underlying event is taken into account event-by-event. The remaining (statistical) region-to-region fluctuations are removed on an ensemble basis by unfolding the jet spectra for different event plane orientations independently. Significant non-zero nu(ch)(2) (jet) is observed in semi-central collisions (30-50% centrality) for 20 < p(T)(ch) (jet) < 90 GeV/c. The azimuthal dependence of the charged jet production is similar to the dependence observed for jets comprising both charged and neutral fragments, and compatible with measurements of the nu(2) of single charged particles at high p(T). Good agreement between the data and predictions from JEWEL, an event generator simulating parton shower evolution in the presence of a dense QCD medium, is found in semi-central collisions.

PHYSICS LETTERS B 753, 511-525, 2016. DOI: 10.1016/j.physletb.2015.12.047

[P022-2016] "Bounds on neutrino-scalar Yukawa coupling"

Pasquini, P. S.*; Peres, O. L. G.*

General neutrino-scalar couplings appear in many extensions of the Standard Model. We can probe these neutrino--scalar couplings by a leptonic decay of mesons and from a heavy neutrino search. Our analysis improves the present limits to vertical bar g(e)vertical bar(2) < 1.9 x 10(-6) and vertical bar g(mu)vertical bar(2) < 1.9 x 10(-7) at 90% C.L. for massless scalars. For massive scalars, we found for the first time the constraints for g(alpha)(2) couplings to be 10(-6) - 10(-1), respectively, for scalar masses between up 100 MeV, and we have no limits for masses above 300 MeV.

PHYSICAL REVIEW D 93[5] 053007, 2016. DOI: 10.1103/PhysRevD.93.053007

[P023-2016] "Bragg Gratings Inscription in Highly Birefringent Microstructured POFs"

Oliveira, R.; Bilro, L.; **Marques, T. H. R.***; Napierala, M.; Tenderenda, T.; Mergo, P.; Nasilowski, T.; **Cordeiro, C. M. B.***; Nogueira, R.

We report for the first time, the fast inscription of high-quality Bragg gratings in highly birefringent microstructured polymer optical fibers by the phase mask method using 248-nm UV radiation. The fibers birefringence is created through a special design of the structure of holes through the fiber. A Bragg grating in these type of fibers allows the creation of two reflection peaks, where the peak separation is related to the phase birefringence.

IEEE PHOTONICS TECHNOLOGY LETTERS 28[6] 621-624, 2016. DOI: 10.1109/LPT.2015.2503241

[P024-2016] "Centrality dependence of pion freeze-out radii in Pb-Pb collisions at root s(NN)=2.76 TeV"

Adam, J.; Adamova, D.; Aggarwal, M. M.; **Chinellato, D. D.*; Dash, A.*; Takahashi, J.***; et al. ALICE Collaboration

We report on the measurement of freeze-out radii for pairs of identical-charge pions measured in Pb-Pb collisions at root s(NN) = 2.76 TeV as a function of collision centrality and the average transverse momentum of the pair k(T). Three-dimensional sizes of the system (femtoscopic radii), as well as direction-averaged one-dimensional radii are extracted. The radii decrease with k(T), following a power-law behavior. This is qualitatively consistent with expectations from a collectively expanding system, produced in hydrodynamic calculations. The radii also scale linearly with < dN(ch)/d eta >(1/3). This behavior is compared to world data on femtoscopic radii in heavy-ion collisions. While the dependence is qualitatively similar to results at smaller root s(NN), a decrease in the ratio R-out/R-side is seen, which is in qualitative agreement with a specific prediction from hydrodynamic models: a change from inside-out to outside-in freeze-out configuration. The results provide further evidence for the production of a collective, strongly coupled system in heavy-ion collisions at the CERN Large Hadron Collider.

PHYSICAL REVIEW C 93[2] 024905, 2016. DOI: 10.1103/PhysRevC.93.024905

[P025-2016] "Centrality evolution of the charged-particle pseudorapidity density over a broad pseudorapidity range in Pb-Pb collisions at root s(NN)=2.76TeV"

Adam, J.; Adamova, D.; Aggarwal, M. M.; **Chinellato, D. D.*; Dash, A.*; Takahashi, J.***; et al. ALICE Collaboration

The centrality dependence of the charged-particle pseudorapidity density measured with ALICE in Pb-Pb collisions at root s(NN) = 2.76 TeV over a broad pseudorapidity range is presented. This Letter extends the previous results reported by ALICE to more peripheral collisions. No strong change of the overall shape of charged-particle pseudorapidity density distributions with centrality is observed, and when normalised to the number of participating nucleons in the collisions, the evolution over pseudorapidity with centrality is likewise small. The broad pseudorapidity range (-3.5 < eta < 5) allows precise estimates of the total number of produced charged particles which we find to range from 162 +/- 22(syst.) to 17170 +/- 770(syst.) in 80-90% and 0-5% central collisions, respectively. The total charged-particle multiplicity is seen to approximately scale with the number of participating nucleons in the collision. This suggests that hard contributions to the charged-particle multiplicity are limited. The results are compared to models which describe dN(ch)/d(eta) at mid-rapidity in the most central Pb-Pb collisions and it is found that these models do not capture all features of the distributions.

PHYSICS LETTERS B 754, 373-385, 2016. DOI: 10.1016/j.physletb.2015.12.082

[P026-2016] "Closed-form expression for the Goos-Hanchen lateral displacement"

Araujo, M. P.*; De Leo, S.; **Maia, G. G.***

The Artmann formula provides an accurate determination of the Goos-Hanchen lateral displacement in terms of the light wavelength, refractive index, and incidence angle. In the total reflection region, this formula is widely used in the literature and confirmed by experiments. Nevertheless, for incidence at critical angle, it tends to infinity and numerical calculations are needed to reproduce the experimental data. In this paper, we overcome the divergence problem at critical angle and find, for Gaussian beams, a closed formula in terms of modified Bessel functions of the first kind. The formula is in excellent agreement with numerical calculations and reproduces, for incidence angles greater than critical ones, the Artmann formula. The closed form also allows one to understand how the breaking of symmetry in the angular distribution is responsible for the difference between measurements done by considering the maximum and the mean value of the beam intensity. The results obtained in this study clearly show the Goos-Hanchen lateral displacement dependence on the angular distribution shape of the incoming beam. Finally, we also present a brief comparison with experimental data and other analytical formulas found in the literature.

PHYSICAL REVIEW A 93[2] 023801, 2016. DOI: 10.1103/PhysRevA.93.023801

[P027-2016] "Comparison of 30 THz impulsive burst time development to microwaves, H alpha, EUV, and GOES soft X-rays"

Miteva, R.; Kaufmann, P.; Cabezas, D. P.; Cassiano, M. M.; Fernandes, L. O. T.; Freeland, S. L.; Karlicky, M.; Kerdraon, A.; Kudaka, A. S.; Luoni, M. L.; **Marcon, R.***; Raulin, J. -P.; Trottet, G.; White, S. M.

The recent discovery of impulsive solar burst emission in the 30 THz band is raising new interpretation challenges. One event associated with a GOES M2 class flare has been observed simultaneously in microwaves, Ha, EUV, and soft X-ray bands. Although these new observations confirm some features found in the two prior known events, they exhibit time profile structure discrepancies between 30 THz, microwaves, and hard X-rays (as inferred from the Neupert effect). These results suggest a more complex relationship between 30 THz emission and radiation produced at other wavelength ranges. The multiple frequency emissions in the impulsive phase are likely to be produced at a common flaring site lower in the chromosphere. The 30 THz burst emission may be either part of a nonthermal radiation mechanism or due to the rapid thermal response to a beam of high-energy particles bombarding the dense solar atmosphere.

ASTRONOMY & ASTROPHYSICS 586, A91, 2016. DOI: 10.1051/0004-6361/201425520

[P028-2016] "Conditional reversibility in nonequilibrium stochastic systems"

Bonanca, M. V. S.*; Jarzynski, C.

For discrete-state stochastic systems obeying Markovian dynamics, we establish the counterpart of the conditional reversibility theorem obtained by Gallavotti for deterministic systems [Ann. de l'Institut Henri Poincare (A) 70, 429 (1999)]. Our result states that stochastic trajectories conditioned on opposite values of entropy production are related by time reversal, in the long-time limit. In other words, the probability of observing a particular sequence of events, given a long trajectory with a specified entropy production rate sigma, is the same as the probability of observing the time-reversed sequence of events, given a trajectory conditioned on the opposite entropy production,-sigma, where both trajectories are sampled from the same underlying Markov process. To obtain our result, we use an equivalence between conditioned ("microcanonical") and biased ("canonical") ensembles of nonequilibrium trajectories. We provide an example to illustrate our findings.

PHYSICAL REVIEW E 93[2] 022101, 2016. DOI: 10.1103/PhysRevE.93.022101

[P029-2016] "Delayed light emission of Tetraphenyl-butadiene excited by liquid argon scintillation light. Current status and future plans"

Segreto, E.*; Machado, A. A.*; Araujo, W.; Teixeira, V.

Tetraphenyl-butadiene is the wavelength shifter most widely used in combination with liquid argon. The latter emits scintillation photons with a wavelength of 127 nm that need to be downshifted to be detected by photomultipliers with glass or quartz windows. Tetraphenyl-butadiene has been demonstrated to have an extremely high conversion efficiency, possibly higher than 100% for 127 nm photons, while there is no precise information about the time dependence of its emission. It is usually assumed to be exponentially decaying with a characteristic time of the order of one ns, as an extrapolation from measurements with exciting radiation in the near UV. This work shows that tetraphenyl-butadiene, when excited by 127 nm photons, re-emits photons not only with a very short decay time, but also with slower ones due to triplet states de-excitations. This fact can strongly contribute to clarifying the anomalies in liquid-argon scintillation light reported in the literature since the 1970s. Precision measurements of the properties of TPB, when excited by Vacuum Ultra Violet photons are being carried on at the Brazilian Synchrotron Light Laboratory in Campinas (State of Sao Paulo).

JOURNAL OF INSTRUMENTATION 11, C02010, 2016. DOI: 10.1088/1748-0221/11/02/C02010

[P030-2016] "Determination of the effective anisotropy constant of CoFe2O4 nanoparticles through the T-dependence of the coercive field"

Carvalho, M. H.; Lima, R. J. S.; Meneses, C. T.; Folly, W. S. D.; Sarmento, V. H. V.; **Coelho, A. A.*;** Duque, J. G. S.

We present a systematic study of the coercive field of CoFe2O4--SiO2 nanocomposites. The samples were prepared via the sol--gel method by using the Tetraethyl Orthosilicate as starting reagent. Results of X-ray diffraction, transmission electron microscopy, and X-ray fluorescence confirm the dispersion of the magnetic nanoparticles inside the silica matrix. In addition, the shift in the maximum of Zero-Field-Cooled curves observed by varying the weight ratio of CoFe2O4 nanoparticles to the precursor of silica is consistent with the increasing of average interparticle distances. Because our samples present a particle size distribution, we have used a generalized model which takes account such parameter to fit the experimental data of coercive field extracted from the magnetization curves as a function of applied field. Unlike most of the coercive field results reported in the literature for this material, the use of this model provided a successful description of the temperature dependence of the coercive field of CoFe2O4 nanoparticles in a wide temperature range. Surprisingly, we have observed the decreasing of the nanoparticles anisotropy constant in comparison to the bulk value expected for the material. We believe that this can be interpreted as due to both the migration of the Co2+ from octahedral to tetrahedral sites.

JOURNAL OF APPLIED PHYSICS 119[9] 093909, 2016. DOI: 10.1063/1.4942535

[P031-2016] "Determination of Young's modulus using optical fiber long-period gratings"

Mosquera, L.*; Osorio, J. H.*; Cordeiro, C. M. B.*

Curvature sensitive CO2-laser induced long-period fiber gratings (LPGs) were employed to measure the Young's moduli of materials. Two techniques, 'bar resonance' and 'through transmission', were used. In the first case, flexural vibrations of bars made of various industrial materials arranged in a cantilever configuration were probed by the LPG. The measured response allowed us to obtain the bar's vertical movement as a function of time, its frequency components and the bar material's Young's modulus. In the second case, the optical response of LPGs was used to determine the propagation velocities of perturbations along a bar, which allowed the straightforward calculation of the Young's modulus. The values obtained show good agreement with the ones reported in the literature. The results obtained in this paper demonstrate the feasibility of using LPGs to dynamically characterize a material's elastic properties. To the best of our knowledge, this is the first demonstration of the use of long-period fiber gratings for dynamically determining Young's modulus values.

MEASUREMENT SCIENCE AND TECHNOLOGY 27[1] 015102, 2016. DOI: 10.1088/0957-0233/27/1/015102

[P032-2016] "Dilution effects in spin 7/2 systems. The case of the antiferromagnet GdRhIn5"

Lora-Serrano, R.; Garcia, D. J.; Betancourth, D.; Amaral, R. P.; Camilo, N. S.; Estevez-Rams, E.; Ortellado G Z, L. A.; **Pagliuso, P. G.***

We report the structural and magnetic characterization of La--substituted Gd(1-x)LaxRhIn(5) (x < 0.50) anti ferromagnetic (AFM) compounds. The magnetic responses of pure GdRhIn5 are well described by a S=7/ 2 Heisenberg model. When Gd3+ ions are substituted by Lai-', the maximum of the susceptibility and the inflection point of the magnetic specific heat are systematically shifted to lower temperatures accompanied by a broadening of the transition. The data is qualitatively explained by a phenomenological model which incorporates a distribution of magnetic regions with different transition temperatures (TN). The universal behaviour of the low temperature specific heat is found for La (vacancies) concentrations below x=0.40 which is consistent with spin wave excitations. For x=0.5 this universal behaviour is lost. The sharp second order transition of GdRhIn5 is destroyed, as seen in the specific heat data, contrary to what is expected for a Heisenberg model. The results are discussed in the context of the magnetic behaviour observed for the La -substituted (Ce,Tb,Nd)Rhln(5) compounds.

JOURNAL OF MAGNETISM AND MAGNETIC MATERIALS 405, 304-310, 2016. DOI: 10.1016/j.jmmm.2015.12.093

[P033-2016] "Diploid versus haploid models of neutral speciation"

Schneider, D. M.*; Baptestini, E. M.*; de Aguiar, M. A. M.*

Neutral models of speciation based on isolation by distance and assortative mating, termed topopatric, have shown to be successful in describing abundance distributions and species-area relationships. Previous works have considered this type of process in the context of haploid genomes. Here we discuss the implementation of two schemes of dominance to analyze the effects of diploidy: a complete dominance model in which one allele dominates over the other and a perfect codominant model in which heterozygous genotypes give rise to a third phenotype. In the case of complete dominance, we observe that speciation requires stronger spatial inbreeding in comparison to the haploid model. For perfect codominance, instead, speciation demands stronger genetic assortativeness. Nevertheless, once speciation is established, the three models predict the same abundance distributions even at the quantitative level, revealing the robustness of the original mechanism to describe biodiversity features.

JOURNAL OF BIOLOGICAL PHYSICS 42[2] 235-245, 2016. DOI: 10.1007/s10867-015-9404-1

[P034-2016] "Direct photon production in Pb-Pb collisions at root s(NN)=2.76 TeV"

Adam, J.; Adamova, D.; Aggarwal, M. M.; **Chinellato, D. D.*; Dash, A*.; Takahashi, J.*;** et al. ALICE Collaboration

Direct photon production at mid-rapidity in Pb-Pb collisions at root s(NN) = 2.76 TeV was studied in the transverse momentum range 0.9 < p(T) < 14 GeV/c. Photons were detected with the highly segmented electromagnetic calorimeter PHOS and via conversions in the ALICE detector material with the e(+)e(-) pair reconstructed in the central tracking system. The results of the two methods were combined and direct photon spectra were measured for the 0-20%, 20-40%, and 40-80% centrality classes. For all three classes, agreement was found with perturbative QCD calculations for p(T) greater than or similar to 5 GeV/c. Direct photon spectra down to p(T) approximate to 1 GeV/c could be extracted for the 20-40% and 0-20% centrality classes. The significance of the direct photon signal for 0.9 < p(T) < 2.1 GeV/c is 2.6 sigma for the 0-20% class. The spectrum in this p(T) range and centrality class can be described by an exponential with an inverse slope parameter of (297 +/- 12(stat) +/- 41(syst)) MeV. State-of-the-art models for photon production in heavy-ion collisions agree with the data within uncertainties.

PHYSICS LETTERS B 754, 235-248, 2016. DOI: 10.1016/j.physletb.2016.01.020

[P035-2016] "Elliptic flow of muons from heavy-flavour hadron decays at forward rapidity in Pb-Pb collisions at root s(NN)=2.76TeV"

Adam, J.; Adamova, D.; Aggarwal, M. M.; **Chinellato, D. D.*; Dash, A.*; Takahashi, J.*;** et al. ALICE Collaboration

The elliptic flow, v(2), of muons from heavy-flavour hadron decays at forward rapidity (2.5 < y < 4) is measured in Pb-Pb collisions at root s(NN)= 2.76TeVwith the ALICE detector at the LHC. The scalar product, two- and four-particle Q cumulants and Lee-Yang zeros methods are used. The dependence of the v(2) of muons from heavy-flavour hadron decays on the collision centrality, in the range 0-40%, and on transverse momentum, p(T), is studied in the interval 3 < p(T)< 10 GeV/c. A positive v(2) is observed with the scalar product and two-particle Q cumulants in semi-central collisions (10-20% and 20-40% centrality classes) for the p(T) interval from 3 to about 5GeV/c with a significance larger than 3 sigma, based on the combination of statistical and systematic uncertainties. The v(2) magnitude tends to decrease towards more central collisions and with increasing pT. It becomes compatible with zero in the interval 6 < p(T)< 10 GeV/c. The results are compared to models describing the interaction of heavy quarks and open heavy-flavour hadrons with the high--density medium formed in high-energy heavy-ion collisions.

PHYSICS LETTERS B 753, 41-56, 2016. DOI: 10.1016/j.physletb.2015.11.059

[P036-2016] "Evaluation of carbon nanoscroll materials for post-combustion CO2 capture"

Daff, T. D.; Collins, S. P.; Dureckova, H.; **Perim, E.***; Skaf, M. S.; **Galvao, D. S.***; Woo, T. K.

Carbon nanoscrolls are similar to multi-walled carbon nanotubes but constructed from rolled graphene sheets into papyrus--like structures. In this work, molecular simulations are used to evaluate the post-combustion CO2 capture properties of nanoscrolls made of graphene, alpha-, beta-, and gamma-graphyne, boron nitride, and three types of carbon nitride. The CO2 uptake capacity, CO2/N-2 selectivity and CO2 working capacity were computed with grand canonical Monte Carlo simulations at conditions relevant to post-combustion CO2 capture. The interlayer spacing of the nanoscrolls was optimized for each property and sheet material. For graphene nanoscrolls, the optimal interlayer spacing of 7.3 angstrom was identified for both the CO2 uptake and selectivity, while for working capacity the optimal interlayer spacing was determined to be 8.6 angstrom. It was found that the CO2 uptake capacity of the materials correlated to the density of the sheets from which they were formed. Nanoscrolls made from graphene and boron nitride, which have the highest number of atoms per unit area, also showed the highest CO2 uptakes. At 0.15 bar CO2, 313 K, graphene and boron nitride nanoscrolls exhibited exceptional CO2 uptake capacities of 7.7 and 8.2 mmol/ g, respectively, while also exhibiting high CO2/ N-2 selectivities of 135 and 153, respectively. Molecular dynamics simulations were used to examine the adsorption kinetics. The simulations showed that an empty graphene nanoscroll with a roll length of 200 angstrom could adsorb CO2 into the center of the roll within 10 ns. Materials with pores that can allow CO2 to pass through, such as graphynes, showed much faster adsorption times.

CARBON 101, 218-225, 2016. DOI: 10.1016/j.carbon.2016.01.072

[P037-2016] "Evaluation of conversion coefficients relating air-kerma to H-star(10) using primary and transmitted x-ray spectra in the diagnostic radiology energy range"

Santos, J. C.; Mariano, L.; **Tomal, A.*;** Costa, P. R.

According to the International Commission on Radiation Units and Measurements (ICRU), the relationship between effective dose and incident air-kerma is complex and depends on the attenuation of x-rays in the body. Therefore, it is not practical to use this quantity for shielding design purposes. This correlation is adopted in practical situations by using conversion coefficients calculated using validated mathematical models by the ICRU. The ambient dose equivalent, H*(10), is a quantity adopted by the IAEA for monitoring external exposure. Dose constraint levels are established in terms of H*(10), while the radiation levels in radiometric surveys are calculated by means of the measurements of air-kerma with ion chambers. The resulting measurements are converted into ambient dose equivalents by conversion factors. In the present work, an experimental study of the relationship between the air--kerma and the operational quantity ambient dose equivalent was conducted using different experimental scenarios. This study was done by measuring the primary x-ray spectra and x-ray spectra transmitted through materials used in dedicated chest radiographic facilities, using a CdTe detector. The air-kerma to ambient dose equivalent conversion coefficients were calculated from these measured spectra. The resulting values of the quantity ambient dose equivalent using these conversion coefficients are more realistic than those available in the literature, because they consider the real energy distribution of primary and transmitted x-ray beams. The maximum difference between the obtained conversion coefficients and the constant value recommended in national and international radiation protection standards is 53.4%. The conclusion based on these results is that a constant coefficient may not be adequate for deriving the ambient dose equivalent.

JOURNAL OF RADIOLOGICAL PROTECTION 36[1] 117-132, 2016. DOI: 10.1088/0952-4746/36/1/117

[P038-2016] "Event generator tunes obtained from underlying event and multiparton scattering measurements"

Khachatryan, V.; Sirunyan, A. M.; Tumasyan, A.; **Chinellato, J.*; Tonelli Manganote, E. J.***; et al. CMS Collaboration

New sets of parameters ("tunes")for the underlying-event (UE) modelling of the PYTHIA8, PYTHIA6 and HERWIG++ MonteCarlo event generators are constructed using different parton distribution functions. Combined fits to CMS UE proton-proton (pp) data at root s = 7 TeV and to UE proton-antiproton (p (P) over bar) data from the CDF experiment at lower root s, are used to study the UE models and constrain their parameters, providing thereby improved predictions for proton-proton collisions at 13 TeV.

In addition, it is investigated whether the values of the parameters obtained from fits to UE observables are consistent with the values determined from fitting observables sensitive to double-parton scattering processes. Finally, comparisons are presented of the UE tunes to "minimum bias" (MB) events, multijet, and Drell-Yan (q (Q) over bar -> Z/gamma* -> lepton-antilepton+jets) observables at 7 and 8 TeV, as well as predictions for MB and UE observables at 13 TeV.

EUROPEAN PHYSICAL JOURNAL C 76 [3] 155, 2016. DOI: 10.1140/epjc/s10052-016-3994-z

[P039-2016] "Expansion of arbitrary electromagnetic fields in terms of vector spherical wave functions"

Moreira, W. L.; Ranha Neves, A. A.; Garbos, M. K.; Euser, T. G.; **Cesar, C. L.***

Since 1908, when Mie reported analytical expressions for the fields scattered by a spherical particle upon incidence of plane-waves, generalizing his analysis for the case of an arbitrary incident wave has been an open question because of the cancellation of the prefactor radial spherical Bessel function. This cancellation was obtained before by our own group for a highly focused beam centered in the objective. In this work, however, we show for the first time how these terms can be canceled out for any arbitrary incident field that satisfies Maxwells equations, and obtain analytical expressions for the beam shape coefficients. We show several examples on how to use our method to obtain analytical beam shape coefficients for: Bessel beams, general hollow waveguide modes and specific geometries such as cylindrical and rectangular. Our method uses the vector potential, which shows the interesting characteristic of being gauge invariant. These results are highly relevant for speeding up numerical calculation of light scattering applications such as the radiation forces acting on spherical particles placed in an arbitrary electromagnetic field, as in an optical tweezers system.

OPTICS EXPRESS 24[3] 2370-2382, 2016. DOI: 10.1364/OE.24.002370

[P040-2016] "Exploring central opacity and asymptotic scenarios in elastic hadron scattering"

Fagundes, D. A.; **Menon, M. J.*; Silva, P. V. R. G.***

In the absence of a global description of the experimental data on elastic and soft diffractive scattering from the first principles of QCD, model-independent analyses may provide useful phenomenological insights for the development of the theory in the soft sector. With that in mind, we present an empirical study on the energy dependence of the ratio X between the elastic and total cross sections; a quantity related to the evolution of the hadronic central opacity. The dataset comprises all the experimental information available on proton proton and antiproton-proton scattering in the c.m. energy interval 5 GeV-8 TeV. Generalizing previous works, we discuss four model-independent analytical parameterizations for X, consisting of sigmoid functions composed with elementary functions of the energy and three distinct asymptotic scenarios: either the standard black disk limit or scenarios above or below that limit. Our two main conclusions are the following: (1) although consistent with the experimental data, the black disk does not represent an unique solution; (2) the data reductions favor a semi-transparent scenario, with asymptotic average value for the ratio (X) over bar = 0.30 +/- 0.12. In this case, within the uncertainty, the asymptotic regime may already be reachedaround 1000 TeV. We present a comparative study of the two scenarios, including predictions for the inelastic channel (diffraction dissociation) and the ratio associated with the total cross-section and the elastic slope. Details on the selection of our empirical ansatz for X and physical aspects related to a change of curvature in this quantity at 80-100 GeV, indicating the beginning of a saturation effect, are also presented and discussed.

NUCLEAR PHYSICS A 946, 194-226, 2016. DOI: 10.1016/j.nuclphysa.2015.11.015

[P041-2016] " Forward-central two-particle correlations in p-Pb collisions at root s(NN)=5.02 TeV"

Adam, J.; Adamova, D.; Aggarwal, M. M.; **Chinellato, D. D.*; Dash, A.*; Takahashi, J.***; et al. ALICE Collaboration

Two-particle angular correlations between trigger particles in the forward pseudorapidity range (2.5 < vertical bar eta vertical bar < 4.0) and associated particles in the central range(vertical bar eta vertical bar < 1.0) are measured with the ALICE detector in p-Pb collisions at a nucleon-nucleon centre-of-mass energy of 5.02 TeV. The trigger particles are reconstructed using the muon spectrometer, and the associated particles by the central barrel tracking detectors. In high-multiplicity events, the double-ridge structure, previously discovered in two-particle angular correlations at midrapidity, is found to persist to the pseudorapidity ranges studied in this Letter. The second-order Fourier coefficients for muons in high-multiplicity events are extracted after jet-like correlations from low-multiplicity events have been subtracted. The coefficients are found to have a similar transverse momentum(p(T)) dependence in p-going (p-Pb) and Pb-going (Pb-p) configurations, with the Pb-going coefficients larger by about 16 +/- 6%, rather independent of p(T) within the uncertainties of the measurement. The data are compared with calculations using the AMPT model, which predicts a different p(T) and eta dependence than observed in the data. The results are sensitive to the parent particle v(2) and composition of reconstructed muon tracks, where the contribution from heavy flavour decays is expected to dominate at p(T) > 2GeV/c.

PHYSICS LETTERS B 753, 126-139, 2016. DOI: 10.1016/j.physletb.2015.12.010

[P042-2016] "Grain size and interfacial interdiffusion influence on the magnetic and dielectric properties of magnetoelectric La0.7Ba0.3MnO3-BaTiO3 composites"

Clabel H, J. L.; Ferri, F. A.; Zabotto, F. L.; Rivera, V. A. G.; Nogueira, I. C.; Garcia, D.; **de Lima, O. F.***; Leite, E. R.; Pereira-da-Silva, M. A.; Cardoso, C. A.

We report on specific features of the dielectric and magnetic properties as well as magnetoelectric coupling coefficients (alpha(ME)) of the La0.7Ba0.3MnO3 (L)-BaTiO3 (B) 2-2 type ceramic composite. The powder of L and B was synthesized by two different methods (solid state reaction and Pechini). Orthorhombic and tetragonal phases were observed for the separated phases L and B of the composite, respectively, for both synthesis methods. The characteristics of grain size and interfacial interdiffusion in the L-B-L composite obtained for different synthesis method were studied, showing that diffusion was a typically physical migration, which can be mainly controlled by the grain size. Anomalies in the observed dielectric behavior are attributed to the internal residual stresses and chemically inhomogeneous regions. The existence of a broad magnetic transition observed in the pure L phase and laminated L-B-L composite was also attributed to its small grain size. A comparison of the maximum transversal (alpha(ME)(31)) and longitudinal (alpha(ME)(33)) ME coupling coefficients, at room temperature, is also shown.

JOURNAL OF MAGNETISM AND MAGNETIC MATERIALS 407, 160-166, 2016. DOI: 10.1016/j.jmmm.2016.01.082

[P043-2016] "Graphene healing mechanisms: A theoretical investigation"

Botari, T.*; Paupitz, R.; **da Silva Autreto, P. A.*; Galvao, D. S.***

Large holes in graphene membranes were recently shown to heal, either at room temperature during a low energy STEM experiment, or by annealing at high temperatures. However, the details of the healing mechanism remain unclear. We carried out fully atomistic reactive molecular dynamics simulations in order to address these mechanisms under different experimental conditions. Our results show that, if a carbon atom source is present, high temperatures can provide enough energy for the carbon atoms to overcome the potential energy barrier and to produce perfect reconstruction of the graphene hexagonal structure. At room temperature, this perfect healing is only possible if the heat effects of the electron beam from STEM experiment are explicitly taken into account. The reconstruction process of a perfect or near perfect graphene structure involves the formation of linear carbon chains, as well as rings containing 5, 6, 7 and 8 atoms with planar (Stone-Wales like) and non-planar (lump like) structures. These results shed light on the healing mechanism of graphene when subjected to different experimental conditions. Additionally, the methodology presented here can be useful for investigating the tailoring and manipulations of other nano-structures.

CARBON 99, 302-309, 2016. DOI: 10.1016/j.carbon.2015.11.070

[P044-2016] "Hidden interactions of sterile neutrinos as a probe for new physics"

Tabrizi, Z*; Peres, O. L. G.*

Recent results from neutrino experiments show evidence for light sterile neutrinos which do not have any Standard Model interactions. In this work, we study the hidden interaction of sterile neutrinos with an "MeV-scale" gauge boson (the nu sHI model) with mass M-X and leptonic coupling g'(l). By performing an analysis on the nu sHI model using the data of the MINOS neutrino experiment, we find that the values above G(X)/G(F) = 92.4 are excluded by more than 2 sigma C.L., where G(F) is the Fermi constant and G(X) is the field strength of the nu sHI model. Using this model, we can also probe other new physics scenarios. We find that the region allowed by the (g-2)(mu) discrepancy is entirely ruled out for MX less than or similar to 100 MeV. Finally, the secret interaction of sterile neutrinos has been to solve a conflict between the sterile neutrinos and cosmology. It is shown here that such an interaction is excluded by MINOS for g'(s) > 1.6 x 10(-2). This exclusion, however, does depend on the value of g'(l).

PHYSICAL REVIEW D 93[5] 053003, 2016. DOI: 10.1103/PhysRevD.93.053003

[P045-2016] "Impact of the intermixed phase and the channel network on the carrier mobility of nanostructured solar cells"

Woellner, C. F.*; Freire, J. A.

We analyzed the impact of the complex channel network of donor and acceptor domains in nanostructured solar cells on the mobility of the charge carriers moving by thermally activated hopping. Particular attention was given to the so called intermixed phase, or interface roughness, that has recently been shown to promote an increase in the cell efficiency. The domains were obtained from a Monte Carlo simulation of a two--species lattice gas. We generated domain morphologies with controllable channel size and interface roughness. The field and density dependence of the carrier hopping mobility in different morphologies was obtained by solving a master equation. Our results show that the mobility decreases with roughness and increases with typical channel sizes. The deleterious effect of the roughness on the mobility is quite dramatic at low carrier densities and high fields. The complex channel network is shown to be directly responsible for two potentially harmful effects to the cell performance: a remarkable decrease of the mobility with increasing field and the accumulation of charge at the domains interface, which leads to recombination losses.

JOURNAL OF CHEMICAL PHYSICS 144[8] 084119, 2016. DOI: 10.1063/1.4942613

[P046-2016] "Influence of chemical doping and hydrostatic pressure on the magnetic properties of Mn1-xFexAs magnetocaloric compounds"

Rocco, D. L.; de Campos, A.; Carvalho, A. Magnus G.; dos Santos, A. O.; da Silva, L. M.; Gama, S.; da Luz, M. S.; von Ranke, P.; de Oliveira, N. A.; **Coelho, A. A.*; Cardoso, L. P.*; Souza, J. A.***

This paper presents the results of an investigation of the magnetic and structural properties of Mn1-xFex As compounds under hydrostatic pressure and chemical doping. The chemical doping was performed by using low Fe doping levels (x = 0, 0.003, 0.006, 0.010, 0.015, and 0.018), which emulates the negative pressure effect on the crystal structure. The results of this approach were compared with the physical pressure effect (hydrostatic pressure from 0 to 2.2 kbar) on the Mn0.997Fe0.003As. Both approaches exhibit the same magnetic behaviors: the T-C and saturation magnetization decrease as the pressure increases; for the highest pressure studied, an orthorhombic antiferromagnetic phase occurs below the critical temperature and coexists with the ferromagnetic hexagonal phase. The equivalence between hydrostatic pressure and chemical doping indicates that the Fe doping only causes structural deformation. In addition, we performed magnetic measurements at high temperature (up to 520 K) on the samples with x = 0 and 0.003 in order to investigate the magnetic behavior above T-C = 310 K. These results, along with structural characterization, clearly show that between T-C and T-t the system is a weak antiferromagnet with short-range order confined only in the ab plane. Finally, using the low- and high-temperature data, the magnetic phase diagrams of the compound under hydrostatic pressure and chemical doping were redrawn.

PHYSICAL REVIEW B 93[5] 054431, 2016. DOI: 10.1103/PhysRevB.93.054431

[P047-2016] "Investigation of NAA and NAAG dynamics underlying visual stimulation using MEGA-PRESS in a functional MRS experiment"

Landim, R. C. G.*; Edden, R. A. E.; Foerster, B.; Li, Li Min; **Covolan, R. J. M.*; Castellano, G.***

N-acetyl-aspartate (NAA) is responsible for the majority of the most prominent peak in H-1-MR spectra, and has been used as diagnostic marker for several pathologies. However, similar to 10% of this peak can be attributed to N-acetyl--aspartyl-glutamate (NAAG), a neuropeptide whose release may be triggered by intense neuronal activation. Separate measurement of NAA and NAAG using MRS is difficult due to large superposition of their spectra. Specifically, in functional MRS (fMRS) experiments, most work has evaluated the sum NM + NAAG, which does not appear to change during experiments. The aim of this work was to design and perform an fMRS experiment using visual stimulation and a spectral editing sequence, MEGA-PRESS, to further evaluate the individual dynamics of NM and NAAG during brain activation. The functional paradigm used consisted of three blocks, starting with a rest (baseline) block of 320 s, followed by a stimulus block (640 s) and a rest block (640 s).

Twenty healthy subjects participated in this study. On average, subjects followed a pattern of NAA decrease and NAAG increase during stimulation, with a tendency to return to basal levels at the end of the paradigm, with a peak NM decrease of-(21 +/- 19)% and a peak NAAG increase of (64 62)% (Wilcoxon test p < 0.05). These results may relate to: 1) the only known NAAG synthesis pathway is from NM and glutamate; 2) a relationship between NAAG and the BOLD response.

MAGNETIC RESONANCE IMAGING 34[3] 239-245, 2016. DOI: 10.1016/j.mri.2015.10.038

[P048-2016] "Light sterile neutrinos"

Gariazzo, S.; Giunti, C.; Laveder, M.; Li, Y. F.; **Zavanin, E. M.***

The theory and phenomenology of light sterile neutrinos at the eV mass scale is reviewed. The reactor, gallium and Liquid Scintillator Neutrino Detector anomalies are briefly described and interpreted as indications of the existence of short-baseline oscillations which require the existence of light sterile neutrinos. The global fits of short-baseline oscillation data in 3 + 1 and 3 + 2 schemes are discussed, together with the implications for beta-decay and neutrinoless double-beta decay. The cosmological effects of light sterile neutrinos are briefly reviewed and the implications of existing cosmological data are discussed. The review concludes with a summary of future perspectives.

JOURNAL OF PHYSICS G-NUCLEAR AND PARTICLE PHYSICS 43[3] 033001, 2016. DOI: 10.1088/0954-3899/43/3/033001

[P049-2016] "Linear and Nonlinear Optical Spectroscopy of Fluoroalkylated BODIPY Dyes"

Koelmel, D. K.; **Hoerner, A.*; Castaneda, J. A.*; Ferencz, J. A. P.***; Bihlmeier, A.; Nieger, M.; Braese, S.; **Padilha, L. A.***

A series of fluoroalkyl-labeled BODIPY dyes have been synthesized with different substituents on the 2- and 6-positions and investigated in terms of their spectroscopic properties. The dyes were decorated with aryl, alkenyl, and alkynyl substituents, respectively. Those substituents are able to expend the dyes' delocalized pi-electron system to different extents. Detailed linear and nonlinear optical spectroscopy methods as well as quantum-chemical calculations have been employed to verify the influence of those different substituents on the electronic distribution and, ultimately, on the molecules' optical properties. From the nonlinear optical measurements, we find that the substituents highly influence the excited-state absorption properties, which could be tuned in wavelength by similar to 100 nm and in magnitude by over 1 order of magnitude, reaching peak values close to 10(-15) cm(2) for one of the alkynyl-containing dyes.

JOURNAL OF PHYSICAL CHEMISTRY C 120[8] 4538-4545, 2016. DOI: 10.1021/acs.jpcc.6b00096

[P050-2016] "Localization properties of photonic modes in disordered nonlinear-Kerr/metamaterial heterostructures"

Reyes-Gomez, E.; Cavalcanti, S. B.; **Oliveira, L. E.***

The localization properties of electromagnetic waves in one-dimensional disordered nonlinear-Kerr/metamaterial heterostructures are investigated. Structural disorder is introduced via a random fluctuation of layer widths of both nonlinear-Kerr and metamaterial slabs composing the photonic heterostructure. For frequency values in the vicinity of the zero-n gap, multiple electromagnetic modes with different transmission lengths are obtained for a given value of the Kerr defocusing nonlinearity power. Maximum-delocalized photonic states, which are associated with high-transmission electromagnetic modes corresponding to gap-soliton waves, are found to be quite sensitive with respect to the degree of disorder. Moreover, we have found that inclusion of absorption effects leads, as expected, to a decreasing of the transmission length.

SUPERLATTICES AND MICROSTRUCTURES 90, 1-7, 2016. DOI: 10.1016/j.spmi.2015.11.028

[P051-2016] "Low temperature transport and thermodynamic properties of the Zintl compound Yb11AlSb9: A new Kondo lattice semiconductor"

Magnavita, E. T.; **Rettori, C.***; Osorio-Guillen, J. M.; Ferreira, F. F.; Mendonca-Ferreira, L.; Avila, M. A.; Ribeiro, R. A.

A thorough transport and thermodynamic investigation of flux-grown single crystals of the ternary Zintl phase Yb-11 AlSb9, combined with first-principles density functional theory calculations, shows that this compound is a metal above T approximate to 100 K and a semiconductor with small hybridization gap at low-T. The general behavior resembles those of Kondo lattice semiconductors, although some of the measured properties are strongly sample dependent, as often seen in hybridized f-electron materials. We thus suggest that Yb-11 AlSb9 can be considered as a new Yb-based Kondo lattice semiconductor joining the family of strongly correlated electron systems.

JOURNAL OF ALLOYS AND COMPOUNDS 669, 60-65, 2016. DOI: 10.1016/j.jallcom.2016.01.206

[P052-2016] "Magnetic Dilution Effects in the Intermetallic Compound GdIn3"

Silva, L. S.; Peixoto, E. B.; Mercena, S. G.; **Coelho, A. A.***; Meneses, C. T.; Duque, J. G. S.

In this work, structural and magnetic data of Y (x) Gd1-xIn3 (0 < x < 0.5) single crystals grown from an In flux are reported. X-ray diffraction measurements carried out at room temperature reveal that all samples belong to cubic global symmetry (space group: Pm3m). Besides, the increasing of yttrium concentration produces a decreasing in the lattice parameter. The T-dependence of the magnetic susceptibility shows a peak which is related with the onset of an antiferromagnetic ordering. We believe that yttrium substitution must be decreasing the strength of interaction among magnetic moments of Gd displacing the magnetic transition into to low temperature region. Finally, MvsH loops measured at 2 K are almost linear independently of yttrium concentration.

JOURNAL OF SUPERCONDUCTIVITY AND NOVEL MAGNETISM 29[2] 423-426, 2016. DOI: 10.1007/s10948-015-3278-0

[P053-2016] "Magnetic properties of GdT2Zn20 (T = Fe, Co) investigated by x-ray diffraction and spectroscopy"

Mardegan, J. R. L.*; Francoual, S.; Fabbris, G.; Veiga, L. S. I.; Strempfer, J.; Haskel, D.; Ribeiro, R. A.; Avila, M. A.; **Giles, C.***

We investigate the magnetic and electronic properties of the GdT2Zn20 (T = Fe and Co) compounds using x-ray resonant magnetic scattering (XRMS), x-ray absorption near-edge structure (XANES), and x-ray magnetic circular dichroism (XMCD). The XRMS measurements reveal that GdCo2Zn20 has a commensurate antiferromagnetic spin structure with a magnetic propagation vector (tau) over right arrow = (1/2, 1/2, 1/2) below the Neel temperature (T-N similar to 5.7 K). Only the Gd ions carry a magnetic moment forming an antiferromagnetic structure with magnetic representation Gamma(6).

For the ferromagnetic GdFe2Zn20 compound, an extensive investigation was performed at low temperature and under magnetic field using XANES and XMCD. A strong XMCD signal of about 12.5% and 9.7% is observed below the Curie temperature (T-C similar to 85K) at the Gd L-2 and L-3 edges, respectively. In addition, a small magnetic signal of about 0.06% of the jump is recorded at the Zn K edge, suggesting that the Zn 4p states are spin polarized by the Gd 5d extended orbitals.

PHYSICAL REVIEW B 93[2] 024421, 2016. DOI: 10.1103/PhysRevB.93.024421

[P054-2016] "Magnetocaloric effect and evidence of superparamagnetism in GdAl2 nanocrystallites: A magnetic-structural correlation"

de Paula, V. G.*; da Silva, L. M.; dos Santos, A. O.; Lang, R.; Otubo, L.; **Coelho, A. A.***; **Cardoso, L. P.***

The correlation between structural and magnetic properties of GdAl2, focusing on the role played by the disorder in magnetic ordering and how it influences the magnetocaloric effect (MCE) are discussed. Micrometric-sized particles, consisting of nanocrystallites embedded in an amorphous matrix, were prepared by a mechanical milling technique and characterized by means of x-ray diffraction, scanning and high-resolution transmission electron microscopy as well as magnetic measurements as a function of an applied external magnetic field and temperature. The results show that the average particle size is just slightly diminished (approximate to 7%) with the milling time (between 3 and 13 h), whereas the average crystallite size undergoes an expressive reduction (approximate to 43%). For long milling times, structural disorders mostly associated with crystallite size singularly affect the magnetic properties, leading to a large tablelike MCE in the temperature range between 30 and 165 K. Below 30 K, nanocrystallites with dimensions below a given critical size cause an enhancement in the magnetic entropy change related to superparamagnetic behavior. In contrast, for low milling times, relative cooling power values are improved. These striking features along with the small magnetic hysteresis observed make the milled GdAl2 a promising material for application in the magnetic refrigeration technology. Finally, a discussion in an attempt to elucidate the origin of the spin-glass states previously reported in the literature for mechanically milled GdAl2 samples for very long times (400 and 1000 h) is presented.

PHYSICAL REVIEW B 93[9] 094427, 2016. DOI: 10.1103/PhysRevB.93.094427

[P055-2016] "Magnetocaloric functional properties of Sm0.6Sr0.4MnO3 manganite due to advanced nanostructured morphology"

Andrade, V. M.; Pedro, S. S.; Caraballo Vivas, R. J.; Rocco, D. L.; Reis, M. S.; Campos, A. P. C.; **Coelho, A. A.*;** Escote, M.; Zenatti, A.; Rossi, A. L.

The magnetocaloric effect (MCE) is the key concept to produce new, advanced, freon-like free, low cost and environmental friendly magnetic refrigerators. Among several potential materials, Sm0.6Sr0.4MnO3 manganite presents one of the highest MCE value in comparison to all other known manganites; however, its studied was only concentrated on the bulk material. To overcame this lack of the information nanoparticles and nanotubes of that highlighted manganite were successfully produced by using a sol gel modified method. High resolution transmission electron microscopy revealed nanoparticle and nanotube diameters of 45 nm and 200 nm, respectively; and, in addition, this technique also showed that the wall of the nanotube is formed by the nanoparticles with 25 nm of diameter. The magnetocaloric potentials, Delta S-M versus T curves, of the nanostructures were obtained and they are broader than the their bulk counterpart. This increases the useful temperature range of a magnetic refrigerator. But also an undesired M-shape profile for the nanotube sample was observed, due to the rising of a super paramagnetic behavior. These results also evidenced the existence of a nanoparticle size threshold below which the advantage to make the transition wider is no longer valid.

MATERIALS CHEMISTRY AND PHYSICS 172, 20-25, 2016. DOI: 10.1016/j.matchemphys.2015.12.013

[P056-2016] "Measurement of differential cross sections for Higgs boson production in the diphoton decay channel in pp collisions at root s=8TeV"

Khachatryan, V.; Sirunyan, A. M.; Tumasyan, A.; **Chinellato, J.*; Tonelli Manganote, E. J.*;** et al. CMS Collaboration

A measurement is presented of differential cross sections for Higgs boson (H) production in pp collisions at root s = 8 TeV. The analysis exploits the H -> gamma gamma decay in data corresponding to an integrated luminosity of 19.7 fb(-1) collected by the CMS experiment at the LHC. The cross section is measured as a function of the kinematic properties of the diphoton system and of the associated jets. Results corrected for detector effects are compared with predictions at next-to-leading order and next-to-next-to-leading order in perturbative quantum chromodynamics, as well as with predictions beyond the standard model. For isolated photons with pseudorapidities vertical bar eta vertical bar < 2.5, and with the photon of largest and next-to-largest transverse momentum (p(T)(gamma)) divided by the diphoton mass m(gamma gamma) satisfying the respective conditions of p(T)(gamma)/m(gamma gamma) > 1/3 and > 1/4, the total fiducial cross section is 32 +/- 10 fb.

EUROPEAN PHYSICAL JOURNAL C 76[1] 13, 2016. DOI: 10.1140/epjc/s10052-015-3853-3

[P057-2016] "Measurement of electrons from heavy-flavour hadron decays in p-Pb collisions at root s(NN)=5.02 TeV"

Adam, J.; Adamova, D.; Aggarwal, M. M.; **Chinellato, D. D.*; Dash, A.*; Takahashi, J.*;** et al. ALICE Collaboration

The production of electrons from heavy-flavour hadron decays was measured as a function of transverse momentum (p(T)) in minimum-bias p-Pb collisions at root s(NN) = 5.02 TeV using the ALICE detector at the LHC. The measurement covers the p(T) interval 0.5 < p(T) < 12 GeV/c and the rapidity range -1.065 < y(cms) < 0.135 in the centre-of-mass reference frame. The contribution of electrons from background sources was subtracted using an invariant mass approach. The nuclear modification factor R-pPb was calculated by comparing the p(T)-differential invariant cross section in p-Pb collisions to a pp reference at the same centre-of-mass energy, which was obtained by interpolating measurements at root s = 2.76 TeV and root s= 7 TeV. The R-pPb is consistent with unity within uncertainties of about 25%, which become larger for p(T) below 1 GeV/c. The measurement shows that heavy-flavour production is consistent with binary scaling, so that a suppression in the high-p(T) yield in Pb-Pb collisions has to be attributed to effects induced by the hot medium produced in the final state. The data in p-Pb collisions are described by recent model calculations that include cold nuclear matter effects.

PHYSICS LETTERS B 754, 81-93, 2016. DOI: 10.1016/j.physletb.2015.12.067

[P058-2016] "Measurement of the charge asymmetry in top quark pair production in pp collisions at root s=8 TeV using a template method"

Khachatryan, V.; Sirunyan, A. M.; Tumasyan, A.; **Chinellato, J. A.*; Tonelli Manganote, E. J.***; et al. CMS Collaboration

The charge asymmetry in the production of top quark and antiquark pairs is measured in proton-proton collisions at a center-of-mass energy of 8 TeV. The data, corresponding to an integrated luminosity of 19.6 fb(-1), were collected by the CMS experiment at the LHC. Events with a single isolated electron or muon, and four or more jets, at least one of which is likely to have originated from hadronization of a bottom quark, are selected. A template technique is used to measure the asymmetry in the distribution of differences in the top quark and antiquark absolute rapidities. The measured asymmetry is A(c)(y) = [0.33 +/- 0.26(stat) +/- 0.33(syst)]%, which is the most precise result to date. The results are compared to calculations based on the standard model and on several beyond-the-standard-model scenarios.

PHYSICAL REVIEW D 93[3] 034014, 2016. DOI: 10.1103/PhysRevD.93.034014

[P059-2016] "Measurement of the Top Quark Pair Production Cross Section in Proton-Proton Collisions at root s=13 TeV"

Khachatryan, V.; Sirunyan, A. M.; Tumasyan, A.; **Chinellato, J. A.*; Tonelli Manganote, E. J.*;** et al. CMS Collaboration

The top quark pair production cross section is measured for the first time in proton-proton collisions at root s = 13 TeV by the CMS experiment at the CERN LHC, using data corresponding to an integrated luminosity of 43 pb(-1). The measurement is performed by analyzing events with at least one electron and one muon of opposite charge, and at least two jets. The measured cross section is 746 +/- 58(stat) +/- 53(syst) +/- 36(lumi) pb, in agreement with the expectation from the standard model.

PHYSICAL REVIEW LETTERS 116[5] 052002, 2016. DOI: 10.1103/PhysRevLett.116.052002

[P060-2016] "Measurement of theta(13) in Double Chooz using neutron captures on hydrogen with novel background rejection techniques"

Abe, Y.; Appel, S.; Abrahao, T.; **Gonzalez, L. F. G.*; Kemp, E.*;** et al. Double Chooz Collaboration

The Double Chooz collaboration presents a measurement of the neutrino mixing angle theta(13) using reactor (nu) over bar (e) observed via the inverse beta decay reaction in which the neutron is captured on hydrogen. This measurement is based on 462.72 live days data, approximately twice as much data as in the previous such analysis, collected with a detector positioned at an average distance of 1050m from two reactor cores. Several novel techniques have been developed to achieve significant reductions of the backgrounds and systematic uncertainties. Accidental coincidences, the dominant background in this analysis, are suppressed by more than an order of magnitude with respect to our previous publication by a multi-variate analysis. These improvements demonstrate the capability of precise measurement of reactor (nu) over bar (e) without gadolinium loading. Spectral distortions from the (nu) over bar (e) reactor flux predictions previously reported with the neutron capture on gadolinium events are confirmed in the independent data sample presented here. A value of sin(2) 2 theta(13) = 0.095(0.039)(+0.039)(stat+syst) is obtained from a fit to the observed event rate as a function of the reactor power, a method insensitive to the energy spectrum shape. A simultaneous fit of the hydrogen capture events and of the gadolinium capture events yields a measurement of sin(2) 2 theta(13) = 0.088 +/- 0.033(stat+syst).

JOURNAL OF HIGH ENERGY PHYSICS 1, 163, 2016. DOI: 10.1007/JHEP01(2016)163

[P061-2016] "Measurement of transverse momentum relative to dijet systems in PbPb and pp collisions at root s(NN)=2.76 TeV"

Khachatryan, V.; Sirunyan, A. M.; Tumasyan, A.; **Chinellato, J.*; Tonelli Manganote, E. J.***; et al. CMS Collaboration

An analysis of dijet events in PbPb and pp collisions is performed to explore the properties of energy loss by partons traveling in a quark-gluon plasma. Data are collected at a nucleon-nucleon center-of-mass energy of 2.76 TeV at the LHC. The distribution of transverse momentum (p(T)) surrounding dijet systems is measured by selecting charged particles in different ranges of p(T) and at different angular cones of pseudorapidity and azimuth. The measurement is performed as a function of centrality of the PbPb collisions, the p(T) asymmetry of the jets in the dijet pair, and the distance parameter R used in the anti-k(T) jet clustering algorithm. In events with unbalanced dijets, PbPb collisions show an enhanced multiplicity in the hemisphere of the subleading jet, with the p(T) imbalance compensated by an excess of low-p(T) particles at large angles from the jet axes.

JOURNAL OF HIGH ENERGY PHYSICS 1, 006, 2016. DOI: 10.1007/JHEP01(2016)006

[P062-2016] "Measurements of t(t)over-bar spin correlations and top quark polarization using dilepton final states in pp collisions at root s=8 TeV"

Khachatryan, V.; Sirunyan, A. M.; Tumasyan, A.; **Chinellato, J.*; Tonelli Manganote, E. J.***; et al. CMS Collaboration

Measurements of the top quark-antiquark (t (t) over bar) spin correlations and the top quark polarization are presented for t (t) over bar pairs produced in pp collisions at root s = 8 TeV. The data correspond to an integrated luminosity of 19.5 fb(-1) collected with the CMS detector at the LHC. The measurements are performed using events with two oppositely charged leptons (electrons or muons) and two or more jets, where at least one of the jets is identified as originating from a bottom quark. The spin correlations and polarization are measured from the angular distributions of the two selected leptons, both inclusively and differentially, with respect to the invariant mass, rapidity, and transverse momentum of the t (t) over bar system. The measurements are unfolded to the parton level and found to be in agreement with predictions of the standard model. A search for new physics in the form of anomalous top quark chromo moments is performed. No evidence of new physics is observed, and exclusion limits on the real part of the chromo-magnetic dipole moment and the imaginary part of the chromo-electric dipole moment are evaluated.

PHYSICAL REVIEW D 93[5] 052007, 2016. DOI: 10.1103/PhysRevD.93.052007

[P063-2016] "MRI Texture Analysis Reveals Deep Gray Nuclei Damage in Amyotrophic Lateral Sclerosis"

de Albuquerque, M.; Anjos, L. G. V.; Tavares de Andrade, H. M.; **de Oliveira, M. S.*; Castellano, G.*; Ribeiro de Rezende, T. J.***; Nucci, A.; Franca Junior, M. C.

BACKGROUND AND PURPOSEAmyotrophic Lateral Sclerosis (ALS) is characterized by extensive corticospinal damage, but extrapyramidal involvement is suggested in pathological studies. Texture analysis (TA) is an image processing technique that evaluates the distribution of gray levels between pixels in a given region of interest (ROI). It provides quantitative data and has been employed in several neurodegenerative disorders. Here, we used TA to investigate possible deep gray nuclei (DGN) abnormalities in a cohort of ALS patients. METHODSThirty-two ALS patients and 32 healthy controls underwent MRI in a 3T scanner. The T1 volumetric sequence was used for DGN segmentation and extraction of 11 texture parameters using the MaZda software. Statistical analyses were performed using the Mann-Whitney non-parametric test, with a significance level set at = 0.025 (FDR-corrected) for TA. RESULTSPatients had significantly higher values for the parameter correlation (CO) in both thalami and in the right caudate nucleus compared to healthy controls. Also, the parameter Inverse Difference Moment or Homogeneity (IDM) presented significantly smaller values in the ALS group in both thalami. CONCLUSIONSTA of T1 weighted images revealed DGN alterations in patients with ALS, namely in the thalami and caudate nuclei.

JOURNAL OF NEUROIMAGING 26[2] 201-206, 2016. DOI: 10.1111/jon.12262

[P064-2016] "Multiconfigurational quantum propagation with trajectory-guided generalized coherent states"

Grigolo, A.*; Viscondi, T. F.; **de Aguiar, M. A. M.***

A generalized version of the coupled coherent states method for coherent states of arbitrary Lie groups is developed. In contrast to the original formulation, which is restricted to frozen-Gaussian basis sets, the extended method is suitable for propagating quantum states of systems featuring diversified physical properties, such as spin degrees of freedom or particle indistinguishability. The approach is illustrated with simple models for interacting bosons trapped in double- and triple-well potentials, most adequately described in terms of SU(2) and SU(3) bosonic coherent states, respectively.

JOURNAL OF CHEMICAL PHYSICS 144[9] 094106, 2016. DOI: 10.1063/1.4942926

[P065-2016] "Multiplicity and transverse momentum evolution of charge-dependent correlations in pp, p-Pb, and Pb--Pb collisions at the LHC"

Adam, J.; Adamova, D.; Aggarwal, M. M.; **Chinellato, D. D.*; Dash, A.*; Takahashi, J.*; et al.** ALICE Collaboration

We report on two-particle charge-dependent correlations in pp, p-Pb, and Pb-Pb collisions as a function of the pseudorapidity and azimuthal angle difference, Delta eta and Delta phi respectively. These correlations are studied using the balance function that probes the charge creation time and the development of collectivity in the produced system. The dependence of the balance function on the event multiplicity as well as on the trigger and associated particle transversemomentum (p(T)) in pp, p-Pb, and Pb-Pb collisions at root s(NN) = 7, 5.02, and 2.76 TeV, respectively, are presented. In the low transverse momentum region, for 0.2 < p(T) < 2.0 GeV/c, the balance function becomes narrower in both Delta eta and Delta phi directions in all three systems for events with higher multiplicity. The experimental findings favor models that either incorporate some collective behavior (e.g. AMPT) or different mechanisms that lead to effects that resemble collective behavior (e.g. PYTHIA8 with color reconnection). For higher values of transverse momenta the balance function becomes even narrower but exhibits no multiplicity dependence, indicating that the observed narrowing with increasing multiplicity at low pT is a feature of bulk particle production.

EUROPEAN PHYSICAL JOURNAL C 76[2] 86, 2016. DOI: 10.1140/epjc/s10052-016-3915-1

[P066-2016] "Nanosecond-level time synchronization of autonomous radio detector stations for extensive air showers"

Aab, A.; Abreu, P.; Aglietta, M.; **Chinellato, J. A.*; Daniel, B.*; Diaz Castro, M. L.*; Dobrigkeit, C.*; Escobar, C. O.*; Fauth, A. C.*; Kemp, E.*; Muller, M. A.*; Pakk Selmi-Dei, D.*; Santos, E.*; Theodoro, V. M.***; et al. Pierre Auger Collaboration

To exploit the full potential of radio measurements of cosmic--ray air showers at MHz frequencies, a detector timing synchronization within 1 ns is needed. Large distributed radio detector arrays such as the Auger Engineering Radio Array (AERA) rely on timing via the Global Positioning System (GPS) for the synchronization of individual detector station clocks. Unfortunately, GPS timing is expected to have an accuracy no better than about 5 ns. In practice, in particular in AERA, the GPS clocks exhibit drifts on the order of tens of ns. We developed a technique to correct for the GPS drifts, and an independent method is used to cross-check that indeed we reach a nanosecond-scale timing accuracy by this correction. First, we operate a "beacon transmitter" which emits defined sine waves detected by AERA antennas recorded within the physics data. The relative phasing of these sine waves can be used to correct for GPS clock drifts. In addition to this, we observe radio pulses emitted by commercial airplanes, the position of which we determine in real time from Automatic Dependent Surveillance Broadcasts intercepted with a software-defined radio. From the known source location and the measured arrival times of the pulses we determine relative timing offsets between radio detector stations. We demonstrate with a combined analysis that the two methods give a consistent timing calibration with an accuracy of 2 ns or better. Consequently, the beacon method alone can be used in the future to continuously determine and correct for GPS clock drifts in each individual event measured by AERA.

JOURNAL OF INSTRUMENTATION 11, P01018, 2016. DOI: 10.1088/1748-0221/11/01/P01018

[P067-2016] "Observation of top quark pairs produced in association with a vector boson in pp collisions at root s=8 TeV"

Khachatryan, V.; Sirunyan, A. M.; Tumasyan, A.; **Chinellato, J.*; Tonelli Manganote, E. J.***; et al. CMS Collaboration

Measurements of the cross sections for top quark pairs produced in association with a W or Z boson are presented, using 8 TeV pp collision data corresponding to an integrated luminosity of 19.5 fb(-1), collected by the CMS experiment at the LHC. Final states are selected in which the associated W boson decays to a charged lepton and a neutrino or the Z boson decays to two charged leptons. Signal events are identified by matching reconstructed objects in the detector to specific final state particles from t (t) over barW or t (t) over barZ decays. The t (t) over barW cross section is measured to be 382(-102)(+117) fb with a significance of 4.8 standard deviations from the background-only hypothesis. The t (t) over barZ cross section is measured to be 242(-55)(+65) fb with a significance of 6.4 standard deviations from the background--only hypothesis. These measurements are used to set bounds on five anomalous dimension-six operators that would affect the t (t) over barW and t (t) over barZ cross sections.

JOURNAL OF HIGH ENERGY PHYSICS 1, 096, 2016. DOI: 10.1007/JHEP01(2016)096

[P068-2016] "On the nature of the solvated electron in ice I-h"

de Koning, M.*; Fazzio, A.; Roque da Silva, A. J.; **Antonelli, A.***

The water-solvated excess electron (EE) is a key chemical agent whose hallmark signature, its asymmetric optical absorption spectrum, continues to be a topic of debate. While nearly all investigation has focused on the liquid-water solvent, the fact that the crystalline-water solvated EE shows a very similar visible absorption pattern has remained largely unexplored. Here, we present spin-polarized density-functional theory calculations subject to periodic boundary conditions of the interplay between an EE and a number of intrinsic lattice defects in ice I-h. Our results show that the optical absorption signatures in the presence of three unsaturated hydrogen bonds (HB) are very similar to those observed experimentally. Its low-energy side can be attributed to transitions between the EE ground state and a single localized excited level, in a picture that is different from that for the liquid solvent, where this portion has been associated with hydrogen-like s -> p excitations. The blue tail, on the other hand, relates to transitions between the EE ground state and delocalized excited states, which is in line with the bound-to-continuum transition interpretations for the EE in liquid water. Finally, we find that, depending on the number of dangling HBs participating in the EE trap, its charge density may spontaneously break the spin degeneracy through exchange interactions with the surrounding electrons, displaying the many-electron quantum nature of the EE problem in ice I-h.

CHEMISTRY CHEMICAL PHYSICS 18[6] 4652-4658, 2016. DOI: 10.1039/c5cp06229b

[P069-2016] "Plasma treatment of poly(dimethylsiloxane) surfaces using a compact atmospheric pressure dielectric barrier discharge device for adhesion improvement"

do Nascimento, F.; Parada, S.; Moshkalev, S.; **Machida, M.***

Results of the treatment of poly(dimethylsiloxane) (PDMS) surfaces using novel atmospheric pressure pulsed dielectric barrier discharge plasmas are presented. Different gases (argon, helium, nitrogen) as well as their mixtures with water vapor were compared in terms of the improvement of adhesion between two PDMS samples after processing by plasma. The plasma was characterized by optical emission spectroscopy to identify the emitting species and determine the plasma temperatures. For all the gases studied, plasma processing resulted in increase of adhesion between PDMS samples if long exposure time (larger than 150 s) is applied. However, for very short treatment times (20 plasma pulses, total processing time about 3 s) the highest efficiency was found for helium plasmas. Water contact angles at PDMS surfaces as function of plasma processing time was analyzed. Atomic force microscopy analysis was performed to show reduction in the surface roughness after plasma treatment, which is likely to be the responsible for increase of the surface contact area and thus the adhesion between two PDMS surfaces. The role of the two mechanisms in the improvement of adhesion (enhanced wettability and changes in the surface morphology), for different time scales, is discussed. Interestingly, for the minimum processing time (20 plasma pulses), the improvement in adhesion and reduction of surface roughness are observed although the changes in the water contact angle are insignificant.

JAPANESE JOURNAL OF APPLIED PHYSICS 55[2] 021602, 2016. DOI: 10.7567/JJAP.55.021602

[P070-2016] "Probing the accuracy of reactive and non-reactive force fields to describe physical and chemical properties of graphene-oxide"

Fonseca, A. F.*; Liang, T.; Zhang, D.; Choudhary, K.; Sinnott, S. B.

Graphene-oxide (GO) has been shown to be a promising material for numerous technological applications. Extensive computational work has been devoted to elucidate the structure, stability and properties of different GO species. As some applications require large GO sizes, classical molecular dynamics simulations are necessary to fully investigate GO properties and behavior. There are few classical force fields parameterized to examine oxidized hydrocarbon compounds, and not all of them are able to simulate GO structures. Here, we present the first comparative study of some GO properties between three classical force fields: Reactive Empirical Bond Order for carbon, hydrogen and oxygen (REBO-CHO), third generation of the Charge Optimized Many Body (COMB3) and Chemistry at HARvard Macromolecular Mechanics (CHARMM) force field. The chemical and physical properties tested include key binding energies, carbon-oxygen bond distances and elastic modulus. When compared to density functional theory calculations or experimental data, the COMB3 reactive force field is shown to provide the best overall results, while REBO-CHO and CHARMM provide good results for certain properties of most GO-systems.

COMPUTATIONAL MATERIALS SCIENCE 114, 236-243, 2016. DOI: 10.1016/j.commatsci.2015.12.030

[P071-2016] "Production of light nuclei and anti-nuclei in pp and Pb-Pb collisions at energies available at the CERN Large Hadron Collider"

Adam, J.; Adamova, D.; Aggarwal, M. M.; **Chinellato, D. D.*; Dash, A.*; Takahashi, J.***; et al. ALICE Collaboration

The production of (anti-) deuteron and (anti-) He-3 nuclei in Pb--Pb collisions at root sNN = 2.76 TeV has been studied using the ALICE detector at the LHC. The spectra exhibit a significant hardening with increasing centrality. Combined blast-wave fits of several particles support the interpretation that this behavior is caused by an increase of radial flow. The integrated particle yields are discussed in the context of coalescence and thermal--statistical model expectations. The particle ratios, He-3 / d and He-3 / p, in Pb-Pb collisions are found to be in agreement with a common chemical freeze-out temperature of T-chem approximate to 156 MeV. These ratios do not vary with centrality which is in agreement with the thermal-statistical model. In a coalescence approach, it excludes models in which nucleus production is proportional to the particle multiplicity and favors those in which it is proportional to the particle density instead. In addition, the observation of 31 anti-tritons in Pb-Pb collisions is reported. For comparison, the deuteron spectrum in pp collisions at root s = 7 TeV is also presented. While the p/p ratio is similar in pp and Pb-Pb collisions, the d/p ratio in pp collisions is found to be lower by a factor of 2.2 than in Pb-Pb collisions.

PHYSICAL REVIEW C 93[2] 024917, 2016. DOI: 10.1103/PhysRevC.93.024917

[P072-2016] "Prototype muon detectors for the AMIGA component of the Pierre Auger Observatory"

Aab, A.; Abreu, P.; Aglietta, M.; **Chinellato, J. A.*; Daniel, B.*; Diaz Castro, M. L.*; Dobrigkeit, C.*; Escobar, C. O.*; Fauth, A. C.*; Kemp, E.*; Muller, M. A.*; Pakk Selmi-Dei, D.*; Santos, E.*; Theodoro, V. M.***; et al. Pierre Auger Collaboration

AMIGA (Auger Muons and Infill for the Ground Array) is an upgrade of the Pierre Auger Observatory to extend its range of detection and to directly measure the muon content of the particle showers. It consists of an infill of surface water-Cherenkov detectors accompanied by buried scintillator detectors used for muon counting. The main objectives of the AMIGA engineering array, referred to as the Unitary Cell, are to identify and resolve all engineering issues as well as to understand the muon-number counting uncertainties related to the design of the detector.

The mechanical design, fabrication and deployment processes of the muon counters of the Unitary Cell are described in this document. These muon counters modules comprise sealed PVC casings containing plastic scintillation bars, wavelength-shifter optical fibers, 64 pixel photomultiplier tubes, and acquisition electronics. The modules are buried approximately 2.25 m below ground level in order to minimize contamination from electromagnetic shower particles. The mechanical setup, which allows access to the electronics for maintenance, is also described in addition to tests of the modules' response and integrity. The completed Unitary Cell has measured a number of air showers of which a first analysis of a sample event is included here.

JOURNAL OF INSTRUMENTATION 11, P02012, 2016. DOI: 10.1088/1748-0221/11/02/P02012

[P073-2016] "Pseudorapidity and transverse-momentum distributions of charged particles in proton-proton collisions at root s=13 TeV"

Adam, J.; Adamova, D.; Aggarwal, M. M.; **Chinellato, D. D.*; Dash, A.*; Takahashi, J.***; et al. ALICE Collaboration

The pseudorapidity (eta) and transverse-momentum (p(T)) distributions of charged particles produced in proton-proton collisions are measured at the centre-of-mass energy root s = 13 TeV. The pseudorapidity distribution in vertical bar eta vertical bar < 1.8 is reported for inelastic events and for events with at least one charged particle in vertical bar eta vertical bar < 1. The pseudorapidity density of charged particles produced in the pseudorapidity region vertical bar eta vertical bar < 0.5 is 5.31 +/- 0.18 and 6.46 +/- 0.19 for the two event classes, respectively. The transverse-momentum distribution of charged particles is measured in the range 0.15 < p(T) < 20 GeV/c and vertical bar eta vertical bar < 0.8 for events with at least one charged particle in vertical bar eta vertical bar < 1. The evolution of the transverse momentum spectra of charged particles is also investigated as a function of event multiplicity. The results are compared with calculations from PYTHIA and EPOS Monte Carlo generators.

PHYSICS LETTERS B 753, 319-329, 2016. DOI: 10.1016/j.physletb.2015.12.030

[P074-2016] "Reconstruction and identification of tau lepton decays to hadrons and nu(tau) at CMS"

Khachatryan, V.; Sirunyan, A. M.; Tumasyan, A.; **Chinellato, J.*; Tonelli Manganote, E. J.***; et al. CMS Collaboration

This paper describes the algorithms used by the CMS experiment to reconstruct and identify tau -> hadrons + nu(tau) decays during Run 1 of the LHC. The performance of the algorithms is studied in proton-proton collisions recorded at a centre-of-mass energy of 8 TeV, corresponding to an integrated luminosity of 19.7 fb(-1). The algorithms achieve an identification efficiency of 50-60%, with misidentification rates for quark and gluon jets, electrons, and muons between per mille and per cent levels.

JOURNAL OF INSTRUMENTATION 11, P01019, 2016. DOI: 10.1088/1748-0221/11/01/P01019

[P075-2016] "Reversal magnetization dependence with the Cr and Fe oxidation states in YFe1-xCrxO3 (0 <= x <= 1) perovskites"

Fabian, F. A.; Pedra, P. P.; **Moura, K. O.***; Duque, J. G. S.; Meneses, C. T.

In this work, we have carried out a detailed study of the magnetic and structural properties of YFe1-xCrxO3 (0 <= x <= 1) samples with orthorhombic structure obtained by co-precipitation method. Analysis of X-ray diffraction data using Rietveld refinement show that all samples present an orthorhombic crystal system with space group Pnma. Besides, we have observed a reduction of unit cell volume with increasing of the Cr concentration. SEM images show the formation of grains of micrometer order. X-ray Absorption near edge spectroscopy (XANES) measurements show a shift of absorption edge which can be indicate there is (i) different oxidation states to Fe and Cr ions and/or (ii) a changing in the point symmetry of Fe and Cr ions to the compounds. The magnetization measurements indicate a continuous decreasing of the magnetic transition temperature as function of chromium doping. The reversal magnetization effect was observed to concentrations around x=0.5. Besides, the deviation of the Curie-Weiss law and a weak ferromagnetic behavior observed at room temperature in the M vs H curves can be attributed to the strong magnetic interactions between the transition metals with different oxidation states.

JOURNAL OF MAGNETISM AND MAGNETIC MATERIALS 408, 94-98, 2016. DOI: 10.1016/j.jmmm.2016.02.029

[P076-2016] "Search for a Higgs boson decaying into gamma*gamma -> ll gamma with low dilepton mass in pp collisions at root s=8 TeV"

Khachatryan, V.; Sirunyan, A. M.; Tumasyan, A.; **Chinellato, J.*; Tonelli Manganote, E. J.***; et al. CMS Collaboration

A search is described for a Higgs boson decaying into two photons, one of which has an internal conversion to a muon or an electron pair (ll gamma). The analysis is performed using proton-proton collision data recorded with the CMS detector at the LHC at a centre-of-mass energy of 8TeV, corresponding to an integrated luminosity of 19.7 fb(-1). The events selected have an opposite-sign muon or electron pair and a high transverse momentum photon. No excess above background has been found in the three-body invariant mass range 120 < m(ll gamma) < 150 GeV, and limits have been derived for the Higgs boson production cross section times branching fraction for the decay H -> gamma*gamma -> ll gamma, where the dilepton invariant mass is less than 20 GeV. For a Higgs boson with m(H) = 125 GeV, a 95% confidence level (CL) exclusion observed (expected) limit is 6.7 (5.9(-1.8)(+2.8)) times the standard model prediction. Additionally, an upper limit at 95% CL on the branching fraction of H -> (J/psi)gamma for the 125 GeV Higgs boson is set at 1.5 x10(-3).

PHYSICS LETTERS B 753, 341-362, 2016. DOI: 10.1016/j.physletb.2015.12.039

[P077-2016] "Search for a very light NMSSM Higgs boson produced in decays of the 125 GeV scalar boson and decaying into tau leptons in pp collisions at root 8=TeV"

Khachatryan, V.; Sirunyan, A. M.; Tumasyan, A.; **Chinellato, J.*; Tonelli Manganote, E. J.***; et al. CMS Collaboration

A search for a very light Higgs boson decaying into a pair of tau leptons is presented within the framework of the next--to-minimal supersymmetric standard model. This search is based on a data set corresponding to an integrated luminosity of 19.7 fb(-1) of proton-proton collisions collected by the CMS experiment at a centre-of-mass energy of 8 TeV. The signal is defined by the production of either of the two lightest scalars, h(1) or h(2), via gluon-gluon fusion and subsequent decay into a pair of the lightest Higgs bosons, a(1) or h(1). The h(1) or h(2) boson is identified with the observed state at a mass of 125 GeV. The analysis searches for decays of the a(1) (h(1)) states into pairs of tau leptons and covers a mass range for the a(1) (h(1)) boson of 4 to 8 GeV.

The search reveals no significant excess in data above standard model background expectations, and an upper limit is set on the signal production cross section times branching fraction as a function of the a(1) (h(1)) boson mass. The 95% confidence level limit ranges from 4.5 pb at m(a1) (m(h1)) = 8 GeV to 10.3 pb at m(a1) (m(h1)) = 5 GeV.

JOURNAL OF HIGH ENERGY PHYSICS 1, 079, 2016. DOI: 10.1007/JHEP01(2016)079

[P078-2016] "Search for correlations between the arrival directions of IceCube neutrino events and ultrahigh-energy cosmic rays detected by the Pierre Auger Observatory and the Telescope Array"

Aartsen, M. G.; Abraham, K.; Ackermann, M.; **Chinellato, J. A.*; Daniel, B.*; Castro, M. L. Diaz;* Dobrigkeit, C.*; Escobar, C. O.*; Fauth, A. C.*; Kemp, E.*; Muller, M. A.*; Selmi-Dei, D. Pakk;* Santos, E.*; Theodoro, V. M.*; et al.** IceCube Collaboration; Pierre Auger Collaboration; Telescope Array Collaboration

This paper presents the results of different searches for correlations between very high-energy neutrino candidates detected by IceCube and the highest-energy cosmic rays measured by the Pierre Auger Observatory and the Telescope Array. We first consider samples of cascade neutrino events and of high-energy neutrino-induced muon tracks, which provided evidence for a neutrino flux of astrophysical origin, and study their cross-correlation with the ultrahigh-energy cosmic ray (UHECR) samples as a function of angular separation. We also study their possible directional correlations using a likelihood method stacking the neutrino arrival directions and adopting different assumptions on the size of the UHECR magnetic deflections. Finally, we perform another likelihood analysis stacking the UHECR directions and using a sample of through-going muon tracks optimized for neutrino point-source searches with sub-degree angular resolution. No indications of correlations at discovery level are obtained for any of the searches performed. The smallest of the p-values comes from the search for correlation between UHECRs with IceCube high-energy cascades, a result that should continue to be monitored.

JOURNAL OF COSMOLOGY AND ASTROPARTICLE PHYSICS 1, 037, 2016. DOI: 10.1088/1475-7516/2016/01/037

[P079-2016] "Search for exotic decays of a Higgs boson into undetectable particles and one or more photons"

Khachatryan, V.; Sirunyan, A. M.; Tumasyan, A.; **Chinellato, J.*; Tonelli Manganote, E. J.*;** et al. CMS Collaboration

A search is presented for exotic decays of a Higgs boson into undetectable particles and one or two isolated photons in pp collisions at a center-of-mass energy of 8 TeV. The data correspond to an integrated luminosity of up to 19.4 fb(-1) collected with the CMS detector at the LHC. Higgs bosons produced in gluon-gluon fusion and in association with a Z boson are investigated, using models in which the Higgs boson decays into a gravitino and a neutralino or a pair of neutralinos, followed by the decay of the neutralino to a gravitino and a photon. The selected events are consistent with the background-only hypothesis, and limits are placed on the product of cross sections and branching fractions. Assuming a standard model Higgs boson production cross section, a 95% confidence level upper limit is set on the branching fraction of a 125 GeV Higgs boson decaying into undetectable particles and one or two isolated photons as a function of the neutralino mass. For this class of models and neutralino masses from 1 to 120 GeV an upper limit in the range of 7 to 13% is obtained. Further results are given as a function of the neutralino lifetime, and also for a range of Higgs boson masses.

PHYSICS LETTERS B 753, 363-388, 2016. DOI: 10.1016/j.physletb.2015.12.017

[P080-2016] "Search for Narrow Resonances Decaying to Dijets in Proton-Proton Collisions at root s=13 TeV"

Khachatryan, V.; Sirunyan, A. M.; Tumasyan, A.; **Chinellato, J.*; Tonelli Manganote, E. J.*;** et al. CMS Collaboration

A search for narrow resonances in proton-proton collisions at root s = 13 TeV is presented. The invariant mass distribution of the two leading jets is measured with the CMS detector using a data set corresponding to an integrated luminosity of 2.4 fb(-1). The highest observed dijet mass is 6.1 TeV. The distribution is smooth and no evidence for resonant particles is observed. Upper limits at 95% confidence level are set on the production cross section for narrow resonances with masses above 1.5 TeV. When interpreted in the context of specific models, the limits exclude string resonances with masses below 7.0 TeV, scalar diquarks below 6.0 TeV, axigluons and colorons below 5.1 TeV, excited quarks below 5.0 TeV, color-octet scalars below 3.1 TeV, and W' bosons below 2.6 TeV. These results significantly extend previously published limits.

PHYSICAL REVIEW LETTERS 116 [7] 071801, 2016. DOI: 10.1103/PhysRevLett.116.071801

[P081-2016] "Search for neutral MSSM Higgs bosons decaying to mu(+) mu(-) in pp collisions at root s=7 and 8 TeV"

Khachatryan, V.; Sirunyan, A. M.; Tumasyan, A.; **Chinellato, J.*; Tonelli Manganote, E. J.*;** et al. CMS Collaboration

Search for neutral Higgs bosons predicted in the minimal supersymmetric standard model (MSSM) for mu(+) mu(-) decay channels is presented. The analysis uses data collected by the CMS experiment at the LHC in proton-proton collisions at centre-of-mass energies of 7 and 8 TeV, corresponding to integrated luminosities of 5.1 and 19.3 fb(-1), respectively. The search is sensitive to Higgs bosons produced either through the gluon fusion process or in association with a b (b) over bar quark pair. No statistically significant excess is observed in the mu(+) mu(-) mass spectrum. Results are interpreted in the framework of several benchmark scenarios, and the data are used to set an upper limit on the MSSM parameter tan beta as a function of the mass of the pseudoscalar A boson in the range from 115 to 300 GeV. Model independent upper limits are given for the product of the cross section and branching fraction for gluon fusion and b quark associated production at root s = 8 TeV. They are the most stringent limits obtained to date in this channel.

PHYSICS LETTERS B 752, 221-246, 2016. DOI: 10.1016/j.physletb.2015.11.042

[P082-2016] "Search for pair production of first and second generation leptoquarks in proton-proton collisions at root s=8 TeV"

Khachatryan, V.; Sirunyan, A. M.; Tumasyan, A.; **Chinellato, J.*; Tonelli Manganote, E. J.*;** et al. CMS Collaboration

A search for pair production of first and second generation leptoquarks is performed in final states containing either two charged leptons and two jets, or one charged lepton, one neutrino and two jets, using proton-proton collision data at root s = 8 TeV. The data, corresponding to an integrated luminosity of 19.7 fb(-1), were recorded with the CMS detector at the LHC. First-generation scalar leptoquarks with masses less than 1010 (850) GeV are excluded for beta = 1.0 (0.5), where beta is the branching fraction of a leptoquark decaying to a charged lepton and a quark. Similarly, second-generation scalar leptoquarks with masses less than 1080 (760) GeV are excluded for beta = 1.0 (0.5). Mass limits are also set for vector leptoquark production scenarios with anomalous vector couplings, and for R-parity violating supersymmetric scenarios of top squark pair production resulting in similar final-state signatures.

These are the most stringent limits placed on the masses of vector leptoquarks and RPV top squarks to date.

PHYSICAL REVIEW D 93[3] 032004, 2016. DOI: 10.1103/PhysRevD.93.032004

[P083-2016] "Search for single production of scalar leptoquarks in proton-proton collisions at root s=8 TeV"

Khachatryan, V.; Sirunyan, A. M.; Tumasyan, A.; **Chinellato, J.*; Tonelli Manganote, E. J.***; et al. CMS Collaboration

A search is presented for the production of both first- and second-generation scalar leptoquarks with a final state of either two electrons and one jet or two muons and one jet. The search is based on a data sample of proton-proton collisions at center-of-mass energy root s = 8 TeV recorded with the CMS detector and corresponding to an integrated luminosity of 19.6 fb(-1). Upper limits are set on both the first- and second-generation leptoquark production cross sections as functions of the leptoquark mass and the leptoquark couplings to a lepton and a quark. Results are compared with theoretical predictions to obtain lower limits on the leptoquark mass. At 95% confidence level, single production of first- generation leptoquarks with a coupling and branching fraction of 1.0 is excluded for masses below 1730 GeV, and second-generation leptoquarks with a coupling and branching fraction of 1.0 is excluded for masses below 530 GeV. These are the best overall limits on the production of first-generation leptoquarks to date.

PHYSICAL REVIEW D 93[3] 032005, 2016. DOI: 10.1103/PhysRevD.93.032005

[P084-2016] "Search for the production of an excited bottom quark decaying to tW in proton-proton collisions at root s=8 TeV"

Khachatryan, V.; Sirunyan, A. M.; Tumasyan, A.; **Chinellato, J.*; Tonelli Manganote, E. J.*;** et al. CMS Collaboration

A search is presented for a singly produced excited bottom quark (b*) decaying to a top quark and a W boson in the all-hadronic, lepton+jets, and dilepton final states in proton-proton collisions at root s = 8 TeV recorded by the CMS experiment at the CERN LHC. Data corresponding to an integrated luminosity of 19.7 fb(-1) are used. No significant excess of events is observed with respect to standard model expectations. We set limits at 95% confidence on the product of the b* quark production cross section and its branching fraction to tW. The cross section limits are interpreted for scenarios including left-handed, right-handed, and vector-like couplings of the b* quark and are presented in the two-dimensional coupling plane based on the production and decay coupling constants. The masses of the left-handed, right-handed, and vector-like b* quark states are excluded at 95% confidence below 1390, 1430, and 1530 GeV, respectively, for benchmark couplings. This analysis gives the most stringent limits on the mass of the b* quark to date.

JOURNAL OF HIGH ENERGY PHYSICS 1, 166, 2016. DOI: 10.1007/jhep01(2016)166

[P085-2016] "Search for vectorlike charge 2/3 T quarks in proton-proton collisions at root(s)=8 TeV"

Khachatryan, V.; Sirunyan, A. M.; Tumasyan, A.; **Chinellato, J.*; Tonelli Manganote, E. J.***; et al. CMS Collaboration

A search for fermionic top quark partners T of charge 2/3 is presented. The search is carried out in proton-proton collisions corresponding to an integrated luminosity of 19.7 fb(-1) collected at a center-of-mass energy of root s = 8 TeV with the CMS detector at the LHC. The T quarks are assumed to be produced strongly in pairs and can decay into tH, tZ, and bW. The search is performed in five exclusive channels: a single-lepton channel, a multilepton channel, two all-hadronic channels optimized either for the bW or the tH decay, and one channel in which the Higgs boson decays into two photons. The results are found to be compatible with the standard model expectations in all the investigated final states. A statistical combination of these results is performed and lower limits on the T quark mass are set. Depending on the branching fractions, lower mass limits between 720 and 920 GeV at 95% confidence level are found. These are among the strongest limits on vectorlike T quarks obtained to date.

PHYSICAL REVIEW D 93[1] 012003, 2016. DOI: 10.1103/PhysRevD.93.012003

[P086-2016] "Search for weakly decaying (Lambda n)over--bar and Lambda Lambda exotic bound states in central Pb--Pb collisions at root S-NN=2.76 TeV"

Adam, J.; Adamova, D.; Aggarwal, M. M.; **Chinellato, D. D.*; Dash, A.*; Takahashi, J.***; et al. ALICE Collaboration

We present results of a search for two hypothetical strange dibaryon states, i.e. the H-dibaryon and the possible (Lambda n) over bar bound state. The search is performed with the ALICE detector in central (0-10%) Pb-Pb collisions at root S-NN = 2.76 TeV, by invariant mass analysis in the decay modes (Lambda n) over bar (d) over bar pi(+) and H-dibaryon -> Lambda p pi(-). No evidence for these bound states is observed. Upper limits are determined at 99% confidence level for a wide range of lifetimes and for the full range of branching ratios. The results are compared to thermal, coalescence and hybrid UrQMD model expectations, which describe correctly the production of other loosely bound states, like the deuteron and the hypertriton.

PHYSICS LETTERS B 752, 267-277, 2016. DOI: 10.1016/j.physletb.2015.11.048

[P087-2016] "Single electron ionization and electron capture cross sections for (C6+, H2O) interaction within the Classical Trajectory Monte Carlo (CTMC) approach"

Tran, H. N.; Dao, D. D.; Incerti, S.; **Bernal, M. A.***; Karamitros, M.; Hao, T. V. Nhan; Dang, T. M.; Francis, Z.

In this work, we present a derivation of cross sections for single ionization and electron capture processes within the Classical Trajectory Monte Carlo (CTMC) approach. Specifically, we have used a potential stemming from an ab initio calculation in Green et al.'s framework to describe the dynamics of the water molecule system. Proposing a modified version of the Classical Over--Barrier (COB) potential, we have found that a cut-off of roughly 28 a.u. on the initial distance of the projectile produced a reasonable accuracy. A global agreement has been obtained in our calculations compared to experimental and other theoretical results for C6+ ion energies ranging from 10 keV/u to 10 MeV/u.

NUCLEAR INSTRUMENTS & METHODS IN PHYSICS RESEARCH SECTION B-BEAM INTERACTIONS WITH MATERIALS AND ATOMS 366, 140-144, 2016. DOI:10.1016/j.nimb.2015.10.017

[P088-2016] "Size-dependent complex dielectric function of Ni, Mo, W, Pb, Zn and Na nanoparticles. Application to sizing"

Muneton Arboleda, D.; Santillan, J. M. J.; Mendoza Herrera, L. J.; **Muraca, D.*;** Schinca, D. C.; Scaffardi, L. B.

This work determines the size dependent metal nanoparticle (NP) dielectric function from a 'top-down' approach using the bulk experimental refractive index as a starting point. Free-electron damping constant (gamma(free)) and plasma frequency (omega(p)) parameters in the Drude model are calculated for nickel (Ni), molybdenum (Mo), tungsten (W), lead (Pb), zinc (Zn) and sodium (Na) using a method developed in our group. Determined gamma(free) and omega(p) parameters allow to develop an expression that improves the precision in reproducing the discrete metal bulk dielectric function in a wide wavelength range (UV-FIR). The bulk dielectric function is modified for describing the nanometric case by adding size corrective terms for free and bound electrons contributions. As an application of this study we characterize Ni spherical NPs synthesized by ultrafast laser ablation of a solid target in water. Using Mie theory together with the size-dependent dielectric function, we theoretically reproduce its experimental extinction spectrum. From this fitting, composition and size distribution of the particles in the colloidal suspension may be derived. Transmission electron microscopy (TEM) results agree with the sizes and structure derived from optical extinction spectroscopy (OES).

JOURNAL OF PHYSICS D-APPLIED PHYSICS 49 [7] 075302, 2016. DOI: 10.1088/0022-3727/49/7/075302

[P089-2016] "Solid-Liquid Self-Adaptive Polymeric Composite"

Dong, P.; Chipara, A. C.; Loya, P.; Yang, Y.; Ge, L.; Lei, S.; Li, B.; **Brunetto, G.*; Machado, L. D.***; Hong, L.; Wang, Q.; Yang, B.; Guo, H.; Ringe, E.; **Galvao, D. S.***; Vajtai, R.; Chipara, M.; Tang, M.; Lou, J.; Ajayan, P. M.

A solid liquid self-adaptive composite (SAC) is synthesized using a simple mixing evaporation protocol, with poly(dimethylsiloxane) (PDMS) and poly(vinylidene fluoride) (PVDF) as active constituents. SAC exists as a porous solid containing a near equivalent distribution of the solid (PVDF) liquid (PDMS) phases, with the liquid encapsulated and stabilized within a continuous solid network percolating throughout the structure. The pores, liquid, and solid phases form a complex hierarchical structure, which offers both mechanical robustness and a significant structural adaptability under external forces. SAC exhibits attractive self-healing properties during tension, and demonstrates reversible self-stiffening properties under compression with a maximum of 7-fold increase seen in the storage modulus. In a comparison to existing self-healing and self-stiffening materials, SAC offers distinct advantages in the ease of fabrication, high achievable storage modulus, and reversibility. Such materials could provide a new class of adaptive materials system with multifunctionality, tunability, and scale-up potentials.

ACS APPLIED MATERIALS & INTERFACES 8,[3] 2142-2147, 2016. DOI: 10.1021/acsami.5b10667

[P090-2016] "Soliton-induced transparency in disordered Kerr-metamaterial heterostructures"

Reyes-Gomez, E.; Cavalcanti, S. B.; **Oliveira, L. E.***

The optical transmission properties of light in one-dimensional disordered nonlinear layered systems with meta-material inclusions are theoretically studied. Layer widths of both nonlinear andmetamaterial slabs are considered as random variables without any correlation between them. A thorough investigation of the influence of disorder in the vicinities of a Bragg gap, a zero-n gap, and a bulk-like longitudinal plasmon-polariton gap is performed. Disorder effects result in a considerable broadness of the transmission peaks as compared with periodic nondisordered structures. It is shown that the Bragg-gap soliton reveals itself as the most robust against disorder.

JOURNAL OF THE OPTICAL SOCIETY OF AMERICA B-OPTICAL PHYSICS 33[3] 320-327, 2016. DOI: 10.1364/JOSAB.33.000320

[P091-2016] "Strain Rate Dependent Shear Plasticity in Graphite Oxide"

Vinod, S.; Tiwary, C. S.; **Machado, L. D.*;** Ozden, S.; Cho, J.; Shaw, P.; Vajtai, R.; **Galvao, D. S.***; Ajayan, P. M.

Graphene oxide film is made of stacked graphene layers with chemical functionalities, and we report that plasticity in the filth can be engineered by strain rate tuning. The deformation behavior and plasticity of such functionalized layered systems is dominated by Shear slip between individual layers and interaction between functional groups. Stress-strain behavior and theoretical models suggest that the deformation is strongly strain rate dependent and undergoes brittle to ductile transition with decreasing strain rate.

NANO LETTERS 16[2] 1127-1131, 2016. DOI: 10.1021/acs.nanolett.5b04346

[P092-2016] "Study of B Meson Production in p plus Pb Collisions at root s(NN)=5.02 TeV Using Exclusive Hadronic Decays"

Khachatryan, V.; Sirunyan, A. M.; Tumasyan, A.; **Chinellato, J.*; Tonelli Manganote, E. J.*;** et al. CMS Collaboration

The production cross sections of the B+, B-0, and B-s(0) mesons, and of their charge conjugates, are measured via exclusive hadronic decays in p + Pb collisions at the center-of-mass energy root s(NN) = 5.02 TeV with the CMS detector at the CERN LHC. The data set used for this analysis corresponds to an integrated luminosity of 34.6 nb(-1). The production cross sections are measured in the transverse momentum range between 10 and 60 GeV/c. No significant modification is observed compared to proton-proton perturbative QCD calculations scaled by the number of incoherent nucleon-nucleon collisions. These results provide a baseline for the study of in-medium b quark energy loss in Pb + Pb collisions.

PHYSICAL REVIEW LETTERS 116[3] 032301, 2016. DOI: 10.1103/PhysRevLett.116.032301

[P093-2016] "Study of cosmic ray events with high muon multiplicity using the ALICE detector at the CERN Large Hadron Collider"

Adam, J.; Adamova, D.; Aggarwal, M. M.; **Chinellato, D. D.*; Dash, A.*; Takahashi, J.***; et al. ALICE Collaboration

ALICE is one of four large experiments at the CERN Large Hadron Collider near Geneva, specially designed to study particle production in ultra-relativistic heavy-ion collisions. Located 52 meters underground with 28 meters of overburden rock, it has also been used to detect muons produced by cosmic ray interactions in the upper atmosphere. In this paper, we present the multiplicity distribution of these atmospheric muons and its comparison with Monte Carlo simulations. This analysis exploits the large size and excellent tracking capability of the ALICE Time Projection Chamber. A special emphasis is given to the study of high multiplicity events containing more than 100 reconstructed muons and corresponding to a muon areal density rho(mu) > 5.9 m(-2). Similar events have been studied in previous underground experiments such as ALEPH and DELPHI at LEP. While these experiments were able to reproduce the measured muon multiplicity distribution with Monte Carlo simulations at low and intermediate multiplicities, their simulations failed to describe the frequency of the highest multiplicity events.

In this work we show that the high multiplicity events observed in ALICE stem from primary cosmic rays with energies above 10(16) eV and that the frequency of these events can be successfully described by assuming a heavy mass composition of primary cosmic rays in this energy range. The development of the resulting air showers was simulated using the latest version of QGSJET to model hadronic interactions. This observation places significant constraints on alternative, more exotic, production mechanisms for these events.

JOURNAL OF COSMOLOGY AND ASTROPARTICLE PHYSICS 1, 032, 2016. DOI: 10.1088/1475-7516/2016/01/032

[P094-2016] "Surface structure determination of black phosphorus using photoelectron diffraction"

de Lima, L. H.*; Barreto, L.*; Landers, R.*; de Siervo, A.*

The atomic structure of single-crystalline black phosphorus is studied using high-resolution synchrotron-based photoelectron diffraction (XPD). The results show that the topmost phosphorene layer in the black phosphorus is slightly displaced compared to the bulk structure and presents a small contraction in the direction perpendicular to the surface. Furthermore, the XPD results show the presence of a small buckling among the surface atoms, in agreement with previously reported scanning tunneling microscopy results. The contraction of the surface layer added to the presence of the buckling indicates a uniformity in the size of the sp(3) bonds between P atoms at the surface.

PHYSICAL REVIEW B 93[3] 035448, 2016. DOI: 10.1103/PhysRevB.93.035448

[P095-2016] "The DarkSide project"

Agnes, P.; Agostino, L.; Albuquerque, I. F. M.; **Segreto, E.*; et al.**

DarkSide is a graded experimental project based on radiopure argon, and is now, and will be, used in direct dark matter searches. The present DarkSide-50 detector, operating at the Gran Sasso National Laboratory, is a dual-phase, 50 kg, liquid argon time-projection-chamber surrounded by an active liquid scintillator veto. It is designed to be background free in 3 years of operation. DS-50 performances, when filled with atmospheric argon, are reported. However DS-50 filled with underground argon, shows impressive reduction of the Ar-39 isotope. The application of this powerful technology in a future generation of the DarkSide program is discussed.

JOURNAL OF INSTRUMENTATION 11, C02051, 2016. DOI: 10.1088/1748-0221/11/02/C02051

[P096-2016] "The transverse momentum dependence of charged kaon Bose-Einstein correlations in the SELEX experiment"

Nigmatkulov, G. A.; Ponosovi, A. K.; Akgun, U.; **Escobar, C. O.***; et al. SELEX Collaboration

We report the measurement of the one-dimensional charged kaon correlation functions using 600 GeV/c Sigma(-), pi(-) and 540 GeV/c p beams from the SELEX (E781) experiment at the Fermilab Tevatron. (KK +/-)-K-+/- correlation functions are studied for three transverse pair momentum, k(T), ranges and parameterized by a Gaussian form. The emission source radii, R, and the correlation strength, lambda, are extracted. The analysis shows a decrease of the source radii with increasing kaon transverse pair momentum for all beam types.

PHYSICS LETTERS B 753, 458-464, 2016. DOI: 10.1016/j.physletb.2015.12.041

[P097-2016] "Topological structures in the Husimi flow"

Veronez, M.*; Aguiar, M. A. M.*

We study the topological properties of the quantum phase space current in the Husimi representation, focusing on the dynamical differences, induced by these properties, between the quantum and the classical flows. We show that the zeros of the Husimi function are stagnation points of the current and have a nonzero topological charge. Due to overall charge conservation, new stagnation points with opposite charge appear in pairs in the Husimi current and they have important roles in dynamical processes. As an example we show the topological effect of the zeros in the transmission rate of a particle through a potential barrier.

JOURNAL OF PHYSICS A-MATHEMATICAL AND THEORETICAL 49[6] 065301, 2016. DOI: 10.1088/1751-8113/49/6/065301

[P098-2016] "Transversal symmetry breaking and axial spreading modification for gaussian optical beams"

Araujo, M. P.*; De Leo, S.; Lima, M.

For a long time, it was believed there was no reason to include the geometrical phase in studying the propagation of gaussian optical beams through dielectric blocks. This can be justified by the fact that the first-order term in the Taylor expansion of this phase is responsible for the lateral shift of the optical beam which is also predicted by ray optics. From this point of view, the geometrical phase can be seen as a purely auxiliary concept. In this paper, we show how the second-order term in the Taylor expansion accounts for the symmetry breaking of the transversal spatial distribution and acts as an axial spreading modifier. These new effects clearly show the importance of the geometrical phase in describing the correct behavior of light. To test our theoretical predictions, we briefly discuss a possible experimental implementation.

JOURNAL OF MODERN OPTICS 63[5] 417-427, 2016. DOI: 10.1080/09500340.2015.1076898

[P099-2016] "Transverse momentum spectra of inclusive b jets in pPb collisions atv root s(NN)=5.02 TeV"

Khachatryan, V.; Sirunyan, A. M.; Tumasyan, A.; **Chinellato, J.*; Tonelli Manganote, E. J.***; et al. CMS Collaboration

We present a measurement of b jet transverse momentum (p(T)) spectra in proton-lead (pPb) collisions using a dataset corresponding to about 35nb(-1) collected with the CMS detector at the LHC. Jets from b quark fragmentation are found by exploiting the long lifetime of hadrons containing a b quark through tagging methods using distributions of the secondary vertex mass and displacement. Extracted cross sections for b jets are scaled by the effective number of nucleon-nucleon collisions and are compared to a reference obtained from PYTHIA simulations of pp collisions. The PYTHIA-based estimate of the nuclear modification factor is found to be 1.22 +/- 0.15 (stat + syst pPb) +/- 0.27 (syst PYTHIA) averaged over all jets with p(T) between 55 and 400 GeV/c and with |eta(lab)| < 2. We also compare this result to predictions from models using perturbative calculations in quantum chromodynamics.

PHYSICS LETTERS B 754, 59-80, 2016. DOI: 10.1016/j.physletb.2016.01.010

[P100-2016] "Unusual diffusive effects on the ESR of Nd3+ ions in the tunable topologically nontrivial semimetal YBiPt"

Lesseux, G. G.*; Garitezi, T. M.*; Rosa, P. F. S.*; Jesus, C. B. R.*; Oseroff, S. B.; Sarrao, J. L.; **Fisk, Z.*; Urbano, R. R.*; Pagliuso, P. G.*; Rettori, C.***

Electron spin resonance (ESR) of diluted Nd3+ ions in the topologically nontrivial semimetallic (TNSM) YBiPt compound is reported. The cubic YBiPt compound is a non-centrosymmetric half Heusler material which crystallizes in the F43m space group. The low temperature Nd3+ ESR spectra showed a g-value of 2.66(4) corresponding to a Gamma(6) cubic crystal field Kramers' doublet ground state. Remarkably, the observed metallic and diffusive (Dysonian) Nd3+ lineshape presented an unusual dependence with grain size, microwave power, Nd3+ concentration and temperature. Moreover, the spin dynamic of the localized Nd3+ ions in YBiPt was found to be characteristic of a phonon-bottleneck regime. It is claimed that, in this regime for YBiPt, phonons are responsible for mediating the diffusion of the microwave energy absorbed at resonance by the Nd3+ ions to the thermal bath throughout the skin depth (delta similar or equal to 15 mu m). We argue that this is only possible because of the existence of highly mobile conduction electrons inside the skin depth of YBiPt that are strongly coupled to the phonons by spin-orbit coupling. Therefore, our unexpected ESR results point to a coexistence of metallic and insulating behaviors within the skin depth of YBiPt. This scenario is discussed in the light of the TNSM properties of this compound.

JOURNAL OF PHYSICS-CONDENSED MATTER 28[12] 125601, 2016. DOI: 10.1088/0953-8984/28/12/125601

[P101-2016] "Water-gated phthalocyanine transistors: Operation and transduction of the peptide-enzyme interaction"

de Oliveira, R. F.; **Merces, L.*;** Vello, T. P.; **Bufon, C. C. B.***

The use of aqueous solutions as the gate medium is an attractive strategy to obtain high charge carrier density (10(12) cm(-2)) and low operational voltages (<1 V) in organic transistors. Additionally, it provides a simple and favorable architecture to couple both ionic and electronic domains in a single device, which is crucial for the development of novel technologies in bioelectronics. Here, we demonstrate the operation of transistors containing copper phthalocyanine (CuPc) thin-films gated with water and discuss the charge dynamics at the CuPc/water interface. Without the need for complex multilayer patterning, or the use of surface treatments, water-gated CuPc transistors exhibited low threshold (100 +/- 20 mV) and working voltages (<1 V) compared to conventional CuPc transistors, along with similar charge carrier mobilities (1.2 +/- 0.2) x 10(-3) cm(2) V-1 s(-1). Several device characteristics such as moderate switching speeds and hysteresis, associated with high capacitances at low frequencies upon bias application (3.4 -12 mu F cm(-2)), indicate the occurrence of interfacial ion doping. Finally, water-gated CuPc OTFTs were employed in the transduction of the biospecific interaction between tripeptide reduced glutathione (GSH) and glutathione S-transferase (GST) enzyme, taking advantage of the device sensitivity and multiparametricity.

ORGANIC ELECTRONICS 31, 217-226, 2016. DOI: 10.1016/j.orgel.2016.01.041

***Autores da comunidade IFGW**

Livro publicado

[L001-2016] MARQUES, F.C.* Física Mecânica. São Paulo: Manole, 2016. v. 1. 332p.

Capítulos de Livros publicados

[Ca001-2016] KLEINKE, M. U.*; FREITAS, L. R. Física Moderna na Escola. In: AYOUB, E.; PRADO, G. V. T.; PRODÓCIMO, E. (Org.). PIBID-Unicamp: interlocuções e ações no contexto de uma necessária política de formação de professores. Campinas SP: Edições Leitura Crítica, 2016, v. 6, p. 17-34.

[Ca002-2016] FRATESCHI, N.C.* Leis de Newton II. In: **Marques, F. G.*** (Org.). Física Mecânica. Barueri - SP: Editora Manole Ltda., 2016, p. 113-140.

***Autores da comunidade IFGW**

Defesas de Dissertações

[D003-2016] "Projeto e fabricação de sondas neurais baseadas em MEMS"
Aluno: André Hernandes Alves Malavazi
Orientador: Prof. Dr. Roberto Ricardo Panepucci
Data: 23/02/2016

[D004-2016] "Uso de técnicas ópticas de difusão para caracterização do acoplamento neurovascular-metabólico em humanos"
Aluno: Alexandre Gomes Pinto
Orientador: Prof. Dr. Rickson Coelho de Mesquita
Data: 26/02/2016

[D005-2016] "Avaliação das incertezas sistemáticas em simulações Monte Carlo do transporte de radiação"
Aluno: Eder Humberto Aguirre Contreras
Orientador: Prof. Dr. Mario Antonio Bernal Rodriguez
Data: 04/03/2016

[D006-2016] "Structure of States Saturating the Bounded Strong Sub-additivity and Quantum Channels"
Aluno: Leandro Raffhael da Silva Mendes
Orientador: Prof. Dr. Marcos César de Oliveira
Data: 21/03/2016

[D007-2016] "Efeitos de tamanho e geometria nas propriedades magnéticas e de hipertermia magnética em nanopartículas de Fe(3)O(4)"
Aluno: Juan Manuel Orozco Henao
Orientador: Prof. Dr. Marcelo Knobel
Data: 26/04/2016

Defesas de Teses

[T005-2016] "Dinâmica Molecular Reativa de Sistemas Nanoestruturados"
Aluno: José Moreira de Sousa
Orientador: Prof. Dr. Douglas Soares Galvão
Data: 18/03/2016

[T006-2016] "Singularidades de fase em luz clássica"
Aluno: Paulo Cesar Aguiar Brandão Filho
Orientador: Prof. Dr. Luiz Eduardo Moreira Carvalho Oliveira
Data: 01/04/2016

[T007-2016] "Medidas diretas do efeito magnetocalórico convencional e anisotrópico por medida do fluxo e calor com dispositivos Peltier"
Aluno: José C B. Monteiro
Orientador: Prof. Dr. Flávio C. G. Gandra
Data: 19/04/2016

[T008-2016] "Investigação do uso de métricas aplicadas a dados de fMRI para a análise da dinâmica cerebral"
Aluno: Luis Carlos Tapia Herrera
Orientador: Profa. Dra. Gabriela Castellano
Data: 06/05/2016

[T009-2016] "Estudo da dinâmica de sistemas quânticos compostos sob a influência de ambientes externos"
Aluno: Gustavo Lázero Deçordi
Orientador: Prof. Dr. Antonio Vidiella Barranco
Data: 12/05/2016

[T010-2016] "Processos de inversão da magnetização em redes de nanofios magnéticos modulados"
Aluno: Luis Carlos Costa Arzuza
Orientador: Prof. Dr. Kleber Roberto Pirota
Data: 25/05/2016

Fonte: Portal IFGW/Pós-graduação - Agenda de Colóquios, Defesas e Seminários.
Disponível em: http://portal.ifi.unicamp.br/pos-graduacao

Acesse o portal Abstracta e faça seu cadastro como leitor, para receber em seu e-mail a notificação de cada novo número do boletim publicado:

<http://abstracta.ifi.unicamp.br>

Abstracta

Instituto de Física
Diretor: Prof. Dr. Newton Cesario Frateschi
Diretor Associado: Prof. Dr. Luís Eduardo Evangelista de Araujo
Universidade Estadual de Campinas - UNICAMP
Cidade Universitária Zeferino Vaz
13083-859 - Campinas - SP - Brasil
e-mail: secdir@ifi.unicamp.br

Publicação

Biblioteca do Instituto de Física Gleb Wataghin
http://portal.ifi.unicamp.br/biblioteca

Diretora Técnica: Sandra Maria Carlos Cartaxo
Coordenador da Comissão de Biblioteca: Prof. Dr. Sandro Guedes de Oliveira

Elaboração
Maria Graciele Trevisan (Bibliotecária)
contato: infobif@ifi.unicamp.br